Parametric soil water retention models: a critical evaluation of expressions for the full moisture range.

Raneem Madi[1], Gerrit Huibert de Rooij[1], Henrike Mielenz[2], Juliane Mai[3]

[1]Dept. Soil Physics, Helmholtz Centre for Environmental Research – UFZ, Halle, Germany

[2]Institute for Crop and Soil Science, Julius Kühn-Institut – JKI, Braunschweig, Germany

[3]Dept. Computational Hydrosystems, Helmholtz Centre for Environmental Research – UFZ, Leipzig, Germany

Correspondence to: Gerrit H. de Rooij (gerrit.derooij@ufz.de)

Keywords: soil physics**,** soil water retention functions, parameter estimation, soil hydraulic conductivity functions, unsaturated zone.

Abstract. Of the many parametric expressions for the soil water retention curve, only a few are suitable for the dry range. Furthermore, expressions for the soil hydraulic conductivity curves associated with these retention functions can exhibit non-physical behavior near saturation. We developed a general criterion that needs to be met by soil water retention parameterizations to ensure physically plausible hydraulic conductivity curves. Only three of the 18 tested parameterizations did not impose any restrictions on the parameters of the most popular conductivity curve parameterization, which includes three functions as special cases. One other retention function required one conductivity parameter to be fixed.

We employed the Shuffled Complex Evolution parameter estimation method with the objective function tailored to various observation methods normally used to obtain retention curve data. We fitted the four parameterizations with physically plausible conductivities as well as the most widely used parameterization. We then compared the performance of the resulting 12 combinations of retention curve and conductivity curve in a numerical study with 999 days of semi-arid atmospheric forcing applied to unvegetated, uniform, 1-m freely draining columns for four textures.

Choosing different parameterizations had a minor effect on evaporation, but cumulative bottom fluxes varied by up to an order of magnitude between them. This highlights the need for a careful selection procedure for the parameterization of the soil hydraulic properties that ideally does not only rely on goodness-of-fit to static soil water retention data but also on observations of the hydraulic conductivity curve made during dynamic flow conditions.

1. Introduction

Numerical solvers of Richards' equation for water flow in unsaturated soils require the soil water retention curve and soil hydraulic curve as descriptors of the soil in which the movement of water should be calculated. Many parametric expressions for the retention curve and fewer for the hydraulic conductivity have been developed for that purpose (see section 2, Durner and Flühler (2005), and Khlosi el al. (2008)).

A brief overview of retention curve parameterizations is given in the following while the references to the parameterizations in question are given in section 2, where their equations are presented. The earliest developed parameterizations focused primarily on the wet end of the curve since this is the most relevant section for agricultural production. Numerical models were struggling with the discontinuity of the first derivative at the air-entry value. Observations with methods relying on hydrostatic equilibrium (Klute, 1986, p. 644-647) typically gave a more smooth shape around the matric potential where the soil started to desaturate as an artefact of the sample height, as was later demonstrated by Liu and Dane (1995). This led to the introduction of parameterizations that yielded a continuously differentiable curve.

The interest in the dry end of the retention curve was triggered by an increased interest in water scarcity issues (e.g. Scanlon et al., 2006; UN-Water, FAO, 2007; UNDP, 2006). For groundwater recharge under deep vadose zones, the dry end of the soil water retention curve affects both slow liquid water movement in film and corner flow (Tuller and Or, 2001; Lebeau and Konrad, 2010) and vapor phase transport (Barnes and Turner, 1998; de Vries and Simmers, 2002). The earlier parameterizations had an asymptote at a small (or even zero) water content. This often gave poor fits in the dry end, and several parameterizations emerged in which the dry branch was represented by a logarithmic function that reached zero water content at some point.

A non-parametric approach was advocated by Iden and Durner (2008). They estimated nodal values of volumetric water content from evaporation experiments and derived a smooth retention curve by cubic Hermite interpolation. They extrapolated the retention function to the dry range and compute a coupled conductivity function based on the Mualem model.

Liu and Dane (1995) were the first to point out that the smoothness of observed curves around the air-entry value could be an artefact related to experimental conditions. Furthermore, it became apparent that a particular parameterization that gave a differentiable curve led to unrealistically large increases of the soil hydraulic conductivity near saturation (Vogel et al., 2000). This was eventually linked to the non-zero slope at saturation (Ippisch et al., 2006), implying the existence of unphysically large pores with air-entry values up to zero. This led to the re-introduction of a discrete air-entry value.

The wealth of parameterizations for the soil water retention curve calls for a robust fitting method applicable to various parameterizations and capable of handling data with different data errors. These errors arise from the various measurement techniques used to acquire data over the full water content range. Parameter fitting codes are available (e.g., Schindler et al., 2015), but they do not fit the parameterizations focusing on the dry end. The first objective of this paper is to introduce an objective function that accounts for varying errors embedded in a shell that allows a wide spectrum of retention function parameterizations to be fitted.

The analysis by Ippisch et al. (2006) of the effect of the shape of the soil water retention curve on the hydraulic conductivity near saturation considered van Genuchten's (1980) parameterization in combination with Mualem's (1976) conductivity model only. Iden et al. (2015) approached the same problem but only examined the conductivity curve. They too focused on the van Genuchten-Mualem configuration only. The analysis of Ippisch et al. (2016) could well have ramifications for other parameterizations. A second objective of this paper therefore is the development of a more general analysis based on Ippisch et al. (2006) and its application to other parameterizations of the retention and conductivity curves.

Several hydraulic conductivity parameterizations that relied only on observations of soil water retention data have been developed (see the review by Mualem, 1992). Their mathematical fundamentals were insightfully discussed by Raats (1992). The functions that have found widespread application in numerical models can be captured by Kosugi's (1999) generalized model. In this paper, we limit ourselves to three parameterizations as special cases of Kosugi's general model, and discuss them in more detail in section 2.

Papers introducing new parameterizations of the soil water retention curve as well as reviews of such parameterizations typically show the quality of the fit to soil water retention data (e.g., van Genuchten, 1980; Rossi and Nimmo, 1994; Khlosi et al., 2008). The role of such parameterizations is to be used in solutions of Richards' equation, usually in the form of a numerical model. Their performance can therefore be assessed through the water content and water fluxes in the soil calculated by the numerical Richards solver. A third objective therefore is to carry out a numerical modeling exercise to examine the differences in soil water fluxes calculated on the basis of various parameterizations by the same model for the same scenario. Should these differences be small, the choice of the parameterizations can be based on convenience. If they are significant, even if the fits to the data are fairly similar, this points to a need of a more thorough selection process to determine the most suitable parameterization.

2. Theory

2.1 Hydraulic conductivity models and their behavior near saturation

The pore architecture of the soil influences its hydraulic behavior, typically described by two curves: the relationship between the amount of water present in the soil pores and the matric potential (termed soil water characteristic or soil water retention curve), and the relationship between the hydraulic conductivity and either matric potential or water content (the soil hydraulic conductivity curve).

Numerous functions have been proposed to describe the soil water retention curve, many of them reviewed below. Fewer functions exist to describe the soil hydraulic conductivity curve. When these rely on the retention parameters, one can use the retention curve to predict the conductivity curve. However, when both retention and conductivity data exist, a single set of parameters does not always fit both curves well, even if both sets of data are used in the fitting process. It may therefore be prudent to attempt to find a retention-conductivity pair of curves that share a number of parameters that could be fitted on retention data only and has additional parameters that only occur in the expression for the hydraulic conductivity.

Various theoretical models exist to determine the unsaturated hydraulic conductivity K [LT^{-1}] as a function

110   of matric potential h [L] or volumetric water content θ from the soil water retention curve (see the Appendix for a list of the variables used in this paper). Hoffmann-Riem et al. (1999) and Kosugi (1999) identified a generalized model that captured the two most widely used hydraulic conductivity models and several others. The formulation according to Kosugi (1999) is:

115
$$K(S_e) = K_s S_e^{\tau} \left(\frac{\int_0^{S_e} |h|^{-\kappa}(x)dx}{\int_0^1 |h|^{-\kappa}(x)dx} \right)^{\gamma} \qquad (1)$$

where the subscript s denotes the value at saturation, x is an integration variable, and γ, κ, and τ are dimensionless shape parameters. The degree of saturation S_e is defined as:

$$S_e(h) = \frac{\theta(h) - \theta_r}{\theta_s - \theta_r} \qquad (2)$$

120

where the subscript r denotes the irreducable value (≥ 0). After a change of variables this gives (Ippisch et al. 2006)

$$K(h) = K(h(S_e)) = \begin{cases} K_s S_e^{\tau} \left(\dfrac{\int_{h_{ae}}^{h(S_e)} |h|^{-\kappa} \dfrac{dS}{dh} dh}{\int_{-\infty}^{\infty} |h|^{-\kappa} \dfrac{dS}{dh} dh} \right)^{\gamma}, & h \leq h_{ae} \\ K_s, & h \geq h_{ae} \end{cases} \qquad (3)$$

125   where h_{ae} [L] is the air-entry value of the soil and S denotes the degree of saturation moving between 0 and the actual value S_e. Note that the value of $S(h)$ and dS/dh are directly related to the soil water retention curve $\theta(h)$ through Eq. (2). Specific models can be found by fixing the parameters: Burdine's (1953) model is obtained with $\gamma = 1$, $\kappa = 2$, and $\tau = 2$, the popular model of Mualem (1976) results with $\gamma = 2$, $\kappa = 1$ and $\tau = 0.5$, and the model of Alexander and Skaggs (1986) requires $\gamma = \kappa = \tau = 1$. When any of these models are used, the soil water retention

130   parameters can be used to predict the conductivity curve if no conductivity data are available and the saturated hydraulic conductivity can be estimated independently (see Jarvis et al., 2002, and references therein). Note that positive values of κ ensure that large pores (emptying at smaller values of $|h|$) contribute more to the overall hydraulic conductivity than small pores, which is physically sound. Parameter γ should be positive as well. Negative values would lead to a switch of the numerator and denominator (which scales the numerator by its

135   maximum value) in Eq. (1), which is illogical. Peters (2014) required that the conductivity curve monotonically

decreases as the soil dries out and derived a minimal value of -2 for τ from that requirement. Indeed, negative values of this parameter have been reported (e.g. Schaap and Leij, 2000), even though the three predictive models mentioned above all have positive values of τ.

140   Driven by the occasionally unrealistic shape of Mualem's (1976) hydraulic conductivity curve near saturation, Ippisch et al. (2006) rigorously analyzed the version of Eq. (3) specific to Mualem's (1976) model. They concluded that the integrand must approach zero near saturation in order to prevent unrealistically large virtual pores dominating the hydraulic conductivity of very wet soils. We generalize their criterion for prohibiting excessively larger pores from dominating the conductivity near saturation for arbitrary parameter values (after converting dS/dh to dθ/dh) by

145

$$\lim_{h \to 0} \left(|h|^{-\kappa} \frac{\mathrm{d}\theta}{\mathrm{d}h} \right) = 0 \qquad (4)$$

This condition is automatically met by retention curves with non-zero air-entry values, but restricts the permissible value of κ if the retention curve has non-zero derivatives at saturation, and couples it to this derivative.

150   Iden et al. (2015) argued that limiting the maximum pore size of the pore-bundle models that gave rise to models of the type of Eq. (1) eliminated the large pores that caused the excessively rapid rise of the hydraulic conductivity near saturation. By only modifying the conductivity function without changing the water retention function, a discrepancy emerges between the retention curve (which reflects the presence of unphysically large pores) and the conductivity curve (which does not). Retention curves with a distinct air-entry value maintain the

155   desired consistency, at the price of having non-continuous derivatives, which may create problems for numerical solvers of Richards' equation.

2.2 Critical evaluation of parametric functions of the soil water retention curve

160   This section summarizes the most popular parameterizations of the soil water retention curve and several lesser-known others that were developed to improve the fit in the dry range or at least eliminate the need for the physically poorly defined residual water content. The physical plausibility of the corresponding conductivity models is verified, thereby maintaining the consistency between the retention and the conductivity curves that would have been lost in Iden et al.'s (2015) approach. In all cases but one, this physical plausibility is checked for the first time.

165   The plausibility check requires that the derivative of each retention curve is determined and the criterion in Eq. (4) is used to define the permissible range for κ. If this range does not include any of the values {1, 2} used by the conductivity models described above, or if the permitted values are non-physical (< 0), the retention model does not have a conductivity model associated with it, which limits its practical value. As above, h denotes the matric potential, which is negative in unsaturated soils. Many of the cited papers adopt this notation for its reciprocal, the

170   suction.

The water retention function of Brooks and Corey (1964) is

$$\theta(h) = \begin{cases} \theta_r + (\theta_s - \theta_r)\left(\dfrac{h}{h_{ae}}\right)^{-\lambda}, & h \leq h_{ae} \\ \theta_s, & h > h_{ae} \end{cases} \tag{5a}$$

175

This equation is referred to as BCO below. The derivative is

$$\frac{\mathrm{d}\theta}{\mathrm{d}h} = \begin{cases} \dfrac{-\lambda(\theta_s - \theta_r)}{h_{ae}}\left(\dfrac{h}{h_{ae}}\right)^{-\lambda-1}, & h \leq h_{ae} \\ 0, & h > h_{ae} \end{cases} \tag{5b}$$

180 where λ is a dimensionless fitting parameter. If θ_r is set to zero, Campbell's (1974) equation is obtained.

The analytical expression for the generalized $K(h)$ function (Eq. 3) for the water retention function of Brooks and Corey (1964) is

$$K(h) = \begin{cases} K_s\left(\dfrac{h(S_e)}{h_{ae}}\right)^{-\lambda\tau} \left\{ \dfrac{\left[\dfrac{\lambda(\theta_s - \theta_r)|h_{ae}|^\lambda}{\kappa + \lambda + 2}|h|^{-\kappa-\lambda}\right]_{-\infty}^{h}}{\left[\dfrac{\lambda(\theta_s - \theta_r)|h_{ae}|^\lambda}{\kappa + \lambda + 2}|h|^{-\kappa-\lambda}\right]_{-\infty}^{h_{ae}}} \right\}^{\gamma} = K_s\left(\dfrac{h_{ae}}{h}\right)^{\lambda(\gamma+\tau)+\gamma\kappa}, & h \leq h_{ae} \\ K_s, & h > h_{ae} \end{cases} \tag{5c}$$

185

Note that the Brooks-Corey retention curve allows all three parameters of the associated conductivity model to be fitted.

The derivative of the Brooks-Corey function is discontinuous at h_{ae}. Hutson and Cass (1987) added a parabolic approximation at the wet end to make the first derivative continuous. For $\theta_r = 0$, they proposed

190

$$\theta(h) = \begin{cases} \theta_s\left(\dfrac{h}{h_{ae}}\right)^{-\lambda}, & h \leq h_i \\ \theta_s\left[1 - \left(\dfrac{h}{h_{ae}}\right)^2 \dfrac{\left(1 - \dfrac{2}{\lambda+2}\right)}{\left(\dfrac{2}{\lambda+2}\right)^{-\frac{2}{\lambda}}}\right], & 0 \geq h > h_i \end{cases} \tag{6a}$$

where h_i [L] is the matric potential at the inflection point, given by:

195
$$h_i = h_{ae}\left(\frac{2}{2-\lambda}\right)^{\frac{1}{\lambda}}. \tag{6b}$$

The derivative is

$$\frac{\mathrm{d}\theta}{\mathrm{d}h} = \begin{cases} -\dfrac{\lambda\theta_s}{h_{ae}}\left(\dfrac{h}{h_{ae}}\right)^{-\lambda-1}, & h \leq h_i \\[4mm] \dfrac{2\theta_s}{h_{ae}}\dfrac{\left(\dfrac{2}{\lambda+2}-1\right)}{\left(\dfrac{2}{\lambda+2}\right)^{-\frac{2}{\lambda}}}\left(\dfrac{h}{h_{ae}}\right), & 0 \geq h > h_i \end{cases}. \tag{6c}$$

200

The parameter h_{ae} no longer is an air-entry value and should be considered a pure fitting parameter. It should be noted that the smooth transition to saturation that this function and several others mimic may at least in part be caused by the non-zero height of the soil cores used in experiments to determine soil water retention curves. At hydrostatic equilibrium, the matric potential along the vertical varies in the soil core, resulting in a differentiable

205 shape of the apparent soil water retention curve, even if the soil in the core has a uniform air-entry value that leads to a locally non-differentiable curve (Liu and Dane, 1995).

The parabolic approximation of Hutson and Cass (1987) leads to the following expression for the term in Eq. (4)

210
$$\lim_{h \to 0} A_1 |h|^{1-\kappa} = 0 \tag{7}$$

where A_1 is a constant. This leads to the requirement that $\kappa < 1$, ruling out the usual models. Although the parabolic approximation in itself does not preclude the existence of a closed-form expression for K, the restriction on κ is quite severe, so we do not pursue this further.

215 Van Genuchten's (1980) formulation is also continuously differentiable:

$$\theta(h) = \theta_r + \left(\theta_s - \theta_r\right)\left(1 + |\alpha h|^n\right)^{-m}, \quad h \leq 0 \tag{8a}$$

where α [L^{-1}], n, and m are shape parameters. This equation is denoted by VGN below. It has the derivative

220

$$\frac{\mathrm{d}\theta}{\mathrm{d}h} = \alpha mn(\theta_s - \theta_r)|\alpha h|^{n-1}\left(1 + |\alpha h|^n\right)^{-m-1}, \quad h \leq 0 \tag{8b}$$

where often m is set equal to $1 - 1/n$.

The limit of the derivative of van Genuchten's (1980) retention curve near saturation is

225

$$\left.\frac{\mathrm{d}\theta}{\mathrm{d}h}\right|_{h=0} = \alpha^n mn(\theta_s - \theta_r)|h|^{n-1} \tag{9}$$

leading to the requirement that $\kappa < n\text{-}1$. For many fine and/or poorly sorted soil textures, n ranges between 1 and 2. Therefore, this restriction can be even more severe than the one required for a parabolic wet end, even excluding

230 Mualem's (1976) conductivity model when $n < 2$. For this reason we refrain from formulating analytical conductivity equations, even though van Genuchten (1980) presented such expressions for Burdine's (1953) and Mualem's (1976) models.

Vogel et al. (2000) presented a modification to improve the description of the hydraulic conductivity near saturation without being aware of the physical explanation of the poor behavior presented later by Ippisch et al.

235 (2006). Their retention function reads

$$\theta(h) = \begin{cases} \theta_r + (\theta_m - \theta_r)\left(1 + |\alpha h|^n\right)^{-m}, & h < h_s \\ \theta_s, & h \geq h_s \end{cases} \tag{10a}$$

where h_s [L] is a fitting parameter close to zero with which θ_m can be defined as

240

$$\theta_m = \theta_r + (\theta_s - \theta_r)\left(1 + |\alpha h_s|^n\right)^{-m} \tag{10b}$$

The derivative is

$$\frac{\mathrm{d}\theta}{\mathrm{d}h} = \begin{cases} \alpha mn(\theta_m - \theta_r)|\alpha h|^{n-1}\left(1 + |\alpha h|^n\right)^{-m-1}, & h < h_s \\ 0, & h \geq h_s \end{cases} \tag{10c}$$

245

Schaap and van Genuchten (2006) reported a value of h_s of $- 4$ cm to work best for a wide range of soils to improve the description of the near-saturated hydraulic conductivity. The parameter h_s should therefore not be viewed as an air-entry value.

250   Although an expression can be derived for $K(h)$ if κ is set to 1 and $m = 1 - 1/n$, we prefer to adopt the formulation by Ippisch et al. (2006), given its solid physical footing. They proposed to introduce an air-entry value and scale the unsaturated portion of the retention curve by its value at the water-entry value:

$$\theta(h) = \begin{cases} \theta_r + (\theta_s - \theta_r)\left(\dfrac{1 + |\alpha h|^n}{1 + |\alpha h_{ae}|^n}\right)^{-m}, & h < h_{ae} \\ \theta_s, & h \geq h_{ae} \end{cases}$$

(11a)

255

with derivative

$$\frac{d\theta}{dh} = \begin{cases} \alpha m n (\theta_s - \theta_r)|\alpha h|^{n-1}\left(1 + |\alpha h_{ae}|^n\right)^m\left(1 + |\alpha h|^n\right)^{-m-1}, & h < h_{ae} \\ 0, & h \geq h_{ae} \end{cases}$$

(11b)

260   With the common restriction of $m = 1 - 1/n$, an expression can be found for $\kappa = 1$ that is slightly more general than Eq. (11) in Ippisch et al. (2006):

$$K(h) = \begin{cases} K_s\left(\dfrac{\theta - \theta_r}{\theta_s - \theta_r}\right)^\tau\left[\dfrac{1 - \left(1 - \dfrac{1}{B(h)}\right)^{\frac{n}{n-1}}}{1 - \left(1 - \dfrac{1}{C}\right)^{\frac{n}{n-1}}}\right]^\gamma \\ = K_s\left(\dfrac{B(h)}{C}\right)^{\tau\left(\frac{1}{n}-1\right)}\left[\dfrac{1 - \left(1 - \dfrac{1}{B(h)}\right)^{\frac{n}{n-1}}}{1 - \left(1 - \dfrac{1}{C}\right)^{\frac{n}{n-1}}}\right]^\gamma, & h < h_{ae} \\ K_s, & h \geq h_{ae} \end{cases}$$

(11c)

where

265

$$B(h) = 1 + |\alpha h|^n$$

(11d)

$$C = 1 + |\alpha h_{ae}|^n$$

(11e)

270   This equation can be used to define conductivity models according to Mualem (1976) and Alexander and Skaggs (1986), which both require that $\kappa = 1$.

None of the retention models discussed so far performs very well in the dry range. Campbell and Shiozawa (1992) introduced a logarithmic section in the dry end to improve the fit in the dry range:

275
$$\theta(h) = \theta_a \left(1 - \frac{\ln|h|}{\ln|h_d|} \right) + A_2 \left(\frac{1}{1+|\alpha h|^4} \right)^m \tag{12a}$$

with derivative

$$\frac{d\theta}{dh} = \frac{\theta_a}{\ln|h_d|}\frac{1}{h} + 4\alpha m A_2 |\alpha h|^3 \left(1+|\alpha h|^4\right)^{-m-1} \tag{12b}$$

280

where θ_a represents the maximum amount of adsorbed water, A_2 is a constant and h_d is the matric potential at oven-dryness, below which the water content is assumed to be zero. The first term in the derivative leads to the requirement that $\kappa < -1$, and therefore no conductivity model can be derived from Eq. (12a).

Rossi and Nimmo (1994) also preferred a logarithmic function over the Brooks-Corey power law at the dry
285   end to better represent the adsorption processes that dominates water retention in dry soils, as opposed to capillary processes in wetter soils. They also implemented a parabolic shape at the wet end as proposed by Hutson and Cass (1987). Rossi and Nimmo (1994) presented two retention models, but only one (the junction model) permitted an analytical expression of the unsaturated hydraulic conductivity. Here, the junction model is presented with and without the parabolic expression for the wet end of the retention curve. With the discontinuous derivative at the air-
290   entry value, the expression reads

$$\theta(h) = \begin{cases} 0, & h \le h_d \\ \theta_s \beta \ln\left(\dfrac{h_d}{h}\right), & h_d < h \le h_j \\ \theta_s \left(\dfrac{h_{ae}}{h}\right)^\lambda, & h_j < h \le h_{ae} \\ \theta_s, & h > h_{ae} \end{cases} \tag{13a}$$

which is denoted RNA below. The derivative is

295

$$\frac{\mathrm{d}\theta}{\mathrm{d}h} = \begin{cases} 0, & h \le h_d \\ \dfrac{\theta_s \beta}{-h}, & h_d < h \le h_j \\ \lambda \theta_s |h_{ae}|^{\lambda} |h|^{-\lambda-1}, & h_j < h \le h_{ae} \\ 0, & h > h_{ae} \end{cases} \tag{13b}$$

Rossi and Nimmo (1994) required the power law and logarithmic branches as well as their first derivatives to be equal at the junction point (θ_j, h_j). With h_d fixed (Rossi and Nimmo found a value of -10^5 m for six out of seven soils and $-5 \cdot 10^5$ m for the seventh), these constraints allow two of the five remaining free parameters to be expressed in terms of the other three. Some manipulation leads to the expressions:

$$\lambda = \frac{1}{\ln|h_d| - \ln|h_j|} \tag{13c}$$

$$\beta = \lambda \left(\frac{h_{ae}}{h_j} \right)^{\lambda} \tag{13d}$$

but other choices are possible. This choice leads to fitting parameters h_{ae}, h_j, and θ_s. The associated conductivity model is

$$K(h) = \begin{cases} 0, & h \le h_d \\ K_s S_e^{\tau} \left\{ \dfrac{\left[-\dfrac{\theta_s \beta}{\kappa} |h|^{-\kappa} \right]_{h_d}^{h}}{\left[-\dfrac{\theta_s \beta}{\kappa} |h|^{-\kappa} \right]_{h_d}^{h_j} - \left[\dfrac{\theta_s \lambda}{\lambda + \kappa} |h_{ae}|^{\lambda} |h|^{-(\lambda+\kappa)} \right]_{h_j}^{h_{ae}}} \right\}^{\gamma} \\ \quad = K_s \left[\beta \ln\left(\dfrac{h_d}{h} \right) \right]^{\tau} \left[\dfrac{E(h)}{E(h_j) + F\left(|h_j|^{-\lambda-\kappa} - |h_{ae}|^{-\lambda-\kappa} \right)} \right]^{\gamma}, & h_d < h \le h_j \\ K_s S_e^{\tau} \left\{ \dfrac{\left[-\dfrac{\theta_s \beta}{\kappa} |h|^{-\kappa} \right]_{h_d}^{h_j} - \left[\dfrac{\theta_s \lambda}{\lambda + \kappa} |h_{ae}|^{\lambda} |h|^{-(\lambda+\kappa)} \right]_{h_j}^{h}}{\left[-\dfrac{\theta_s \beta}{\kappa} |h|^{-\kappa} \right]_{h_d}^{h_j} - \left[\dfrac{\theta_s \lambda}{\lambda + \kappa} |h_{ae}|^{\lambda} |h|^{-(\lambda+\kappa)} \right]_{h_j}^{h_{ae}}} \right\}^{\gamma} \\ \quad = K_s \left(\dfrac{h_{ae}}{h} \right)^{\lambda\tau} \left[\dfrac{E(h_j) + F\left(|h_j|^{-\lambda-\kappa} - |h|^{-\lambda-\kappa} \right)}{E(h_j) + F\left(|h_j|^{-\lambda-\kappa} - |h_{ae}|^{-\lambda-\kappa} \right)} \right]^{\gamma}, & h_j < h \le h_{ae} \\ K_s, & h > h_{ae} \end{cases} \tag{13e}$$

310   where

$$E(h) = \frac{\beta}{\kappa}\left(\left|h_d\right|^{-\kappa} - \left|h\right|^{-\kappa}\right)$$
(13f)

$$F = \frac{\lambda}{\lambda + \kappa}\left|h_{ae}\right|^{\lambda}$$
(13g)

315

The junction model of Rossi and Nimmo (1994) with a continuous first-order derivative achieved through the correction by Hutson and Cass (1987) reads

$$\theta(h) = \begin{cases} 0, & h \leq h_d \\ \theta_s \zeta_1 \ln\left(\dfrac{h_d}{h}\right), & h_d < h \leq h_j \\ \theta_s \left(\dfrac{h_{ae}}{h}\right)^{\lambda}, & h_j < h \leq h_i \\ \theta_s\left[1 - c_1\left(\dfrac{h}{h_c}\right)^2\right], & h_i \leq h \leq 0 \end{cases}$$
(14a)

320

with the derivative

$$\frac{d\theta}{dh} = \begin{cases} 0, & h \leq h_d \\ \dfrac{\theta_s \zeta_1}{-h}, & h_d < h \leq h_j \\ \lambda \theta_s \left|h_{ae}\right|^{\lambda}\left|h\right|^{-\lambda - 1}, & h_j < h \leq h_i \\ \dfrac{-2 c_1 \theta_s}{h_c^2}h, & h_i \leq h \leq 0 \end{cases}$$
(14b)

325   where

$$h_i = h_c\left(\frac{\lambda}{2} + 1\right)^{\frac{1}{\lambda}}$$
(14c)

$$h_j = h_d e^{-\frac{1}{\lambda}}$$
(14d)

$$c_1 = \frac{\lambda}{2}\left(\frac{2}{\lambda+2}\right)^{\frac{\lambda+2}{\lambda}} \tag{14e}$$

330

$$\zeta_1 = e\lambda\left(\frac{h_c}{h_d}\right)^{\lambda} \tag{14f}$$

where h_c [L] is a fitting parameter, together with λ and θ_s. The parabolic wet end restricts κ to values between 0 and 1. For this reason, an expression for the conductivity curve is not derived.

335   Rossi and Nimmo (1994) also introduced an equation that summed up the power law and logarithmic contributions (the sum model):

$$\theta(h) = \begin{cases} 0, & h \le h_d \\ \theta_s\left[\left(\frac{h_c}{h}\right)^{\lambda} - \left(\frac{h_c}{h_d}\right)^{\lambda} + \zeta_2 \ln\left(\frac{h_d}{h}\right)\right], & h_d \le h \le h_i \\ \theta_s\left[1 - c_2\left(\frac{h}{h_c}\right)^2\right], & h_i \le h \le 0 \end{cases} \tag{15a}$$

340 with derivative

$$\frac{d\theta}{dh} = \begin{cases} 0, & h \le h_d \\ -\frac{\theta_s}{h}\left[\lambda\left(\frac{h_c}{h}\right)^{\lambda} + \zeta_2\right], & h_d \le h \le h_i \\ \frac{-2c_2\theta_s}{h_c^2}h, & h_i \le h \le 0 \end{cases} \tag{15b}$$

in which we have

345

$$\zeta_2 = \left[1 - \left(\frac{\lambda}{2} + 1\right)\left(\frac{h_c}{h_i}\right)^{\lambda} + \left(\frac{h_c}{h_d}\right)^{\lambda}\right]\left[\frac{1}{2} + \ln\left(\frac{h_d}{h_i}\right)\right]^{-1} \tag{15c}$$

and

$$c_2 = \left(\frac{h_c}{h_i}\right)^2 \left[1 - \left(\frac{h_c}{h_i}\right)^\lambda + \left(\frac{h_c}{h_d}\right)^\lambda - \frac{1 - \left(\frac{\lambda}{2}+1\right)\left(\frac{h_c}{h_i}\right)^\lambda + \left(\frac{h_c}{h_d}\right)^\lambda}{\frac{1}{2\ln\left(\frac{h_d}{h_i}\right)}+1}\right]$$

(15d)

350

A closed-form expression for the hydraulic conductivity does not exist for this function, and the permitted values for κ are not physically acceptable.

Fayer and Simmons (1995) used the approach of Campbell and Shiozawa (1992) to have separate terms for adsorbed and capillary bound water. If the capillary binding is represented by a Brooks-Corey type function, the

355 retention model becomes

$$\theta(h) = \begin{cases} 0, & h \le h_d \\ \theta_a\left(1 - \frac{\ln|h|}{\ln|h_d|}\right) + \left[\theta_s - \theta_a\left(1 - \frac{\ln|h|}{\ln|h_d|}\right)\right]\left(\frac{h_{ae}}{h}\right)^\lambda, & h_d < h < h_{ae} \\ \theta_s, & h \ge h_{ae} \end{cases}$$

(16a)

This expression is denoted FSB below. The derivative is

360

$$\frac{d\theta}{dh} = \begin{cases} 0, & h \le h_d \\ \frac{1}{|h|}\left(\frac{h_{ae}}{h}\right)^\lambda\left[\lambda(\theta_s - \theta_a) + \theta_a\left(\frac{\ln|h|}{\ln|h_d|} - \frac{1}{\ln|h_d|}\right)\right], & h_d < h < h_{ae} \\ 0, & h \ge h_{ae} \end{cases}$$

(16b)

The corresponding conductivity model is

365

$$K(h) = \begin{cases} 0, & h \le h_d \\[4pt] K_s S_e^{\tau} \left\{ \dfrac{\left[\dfrac{|h_{ae}|^{\lambda}}{\ln|h_d|(\lambda+\kappa)} \left[\theta_a\left(\dfrac{\lambda+\kappa-1}{\lambda+\kappa} - \ln|h| \right) - \lambda(\theta_s - \theta_a)\ln|h_d| \right] |h|^{-\lambda-\kappa} \right]_{h_d}^{h}}{\left[\dfrac{|h_{ae}|^{\lambda}}{\ln|h_d|(\lambda+\kappa)} \left[\theta_a\left(\dfrac{\lambda+\kappa-1}{\lambda+\kappa} - \ln|h| \right) - \lambda(\theta_s - \theta_a)\ln|h_d| \right] |h|^{-\lambda-\kappa} \right]_{h_d}^{h_{ae}}} \right\}^{\gamma} & \\[4pt] = K_s \left\{ \dfrac{\theta_a}{\theta_s}\left(1 - \dfrac{\ln|h|}{\ln|h_d|} \right) + \left[1 - \dfrac{\theta_a}{\theta_s}\left(1 - \dfrac{\ln|h|}{\ln|h_d|} \right) \right] \left(\dfrac{h_{ae}}{h} \right)^{\lambda} \right\}^{\tau} & \\[4pt] \left\{ \dfrac{\left[\theta_a(G - \ln|h|) - I \right]|h|^{-\lambda-\kappa} - J}{\left[\theta_a(G - \ln|h_{ae}|) - I \right]|h_{ae}|^{-\lambda-\kappa} - J} \right\}^{\gamma}, & h_d < h \le h_{ae} \\[4pt] K_s, & h \ge h_{ae} \end{cases}$$

(16c)

where

$$G = \frac{\lambda+\kappa-1}{\lambda+\kappa} \tag{16d}$$

370

$$I = \lambda(\theta_s - \theta_a)\ln|h_d| \tag{16e}$$

$$J = \left[\theta_a(G - \ln|h_d|) - I \right] h_d |^{-\lambda-\kappa} \tag{16f}$$

375 Note that the above model is valid if h_{ae} does not exceed -1 cm. This condition will usually be met, unless the soil texture is very coarse.

If capillary binding is described by a van Genuchten function, the resulting equation is

$$\theta(h) = \begin{cases} 0, & h \le h_d \\[4pt] \theta_a\left[1 - \dfrac{\ln|h|}{\ln|h_d|} \right] + \left\{ \theta_s - \theta_a\left[1 - \dfrac{\ln|h|}{\ln|h_d|} \right] \right\} \left[1 + (-\alpha h)^n \right]^{\frac{1}{n}-1}, & h_d < h < 0 \end{cases}$$

(17a)

380

with derivative

$$\frac{d\theta}{dh} = \begin{cases} 0, & h \le h_d \\ \dfrac{\theta_a}{h\ln|h_d|}\left\{\left[1+(-\alpha h)^n\right]^{\frac{1}{n}-1}-1\right\} & \\ +\alpha(1-n)(-\alpha h)^{n-1}\left[1+(-\alpha h)^n\right]^{\frac{1}{n}-2}\left\{\theta_a\left[1-\dfrac{\ln|h|}{\ln|h_d|}\right]-\theta_s\right\}, & h_d < h < 0 \end{cases} \tag{17b}$$

385   The derivative has several terms that pose severe restrictions on the value of κ (the first term even requires that $\kappa < -1$), and other terms that limit the permitted values of n. The conductivity function is therefore omitted here.

In the original equations of both versions as presented by Fayer and Simmons (1995), the adsorbed water content reached zero at h_d, while there is still some capillary bound water at and below that matric potential, which is inconsistent. Furthermore, the terms with ratios of logarithms become negative for matric potentials below h_d. We

390   therefore modified the original equations by setting the water content to zero below h_d.

Kosugi (1996) and Kosugi (1999) presented a soil water retention curve for soils with a lognormal pore size distribution. Khlosi et al. (2008) extended the approach of Campbell and Schiozawa (1992) and Fayer and Simmons (1995) to Kosugi's (1996, 1999) model. We again set the water content to zero for matric potentials below h_d:

395    $$\theta(h) = \begin{cases} 0, & h \le h_d \\ \theta_a\left(1-\dfrac{\ln|h|}{\ln|h_d|}\right)+\left[\theta_s-\theta_a\left(1-\dfrac{\ln|h|}{\ln|h_d|}\right)\right]\dfrac{1}{2}\mathrm{erfc}\left[\dfrac{\ln\left(\dfrac{h}{h_m}\right)}{\sigma\sqrt{2}}\right], & h_d < h < 0 \end{cases} \tag{18a}$$

with the derivative (see Olver et al., 2010, p. 163 and p. 443)

$$\frac{d\theta}{dh} = \begin{cases} 0, & h \le h_d \\ \dfrac{\theta_a}{h\ln|h_d|}\left\{\dfrac{1}{2}\mathrm{erfc}\left[\dfrac{\ln\left(\dfrac{h}{h_m}\right)}{\sigma\sqrt{2}}\right]-1\right\}+\dfrac{\theta_a\left(1-\dfrac{\ln|h|}{\ln|h_d|}\right)-\theta_s}{h\sigma\sqrt{2\pi}}\exp\left\{-\left[\dfrac{\ln\left(\dfrac{h}{h_m}\right)}{\sigma\sqrt{2}}\right]^2\right\}, & h_d < h < 0 \end{cases} \tag{18b}$$

400

Parameter h_m [L] represents the matric potential corresponding to the median pore size, and σ characterizes the width of the pore size distribution. The behavior of the derivative near saturation is not readily clear. Expressions for the corresponding hydraulic conductivity function can only be found for integer values of κ. For $\kappa = 1$, the expression for the hydraulic conductivity is

405

$$
K(h) = \begin{cases}
0, & h \le h_d \\[2ex]
K_s S_e^{\tau} \left\{ \dfrac{\left[\dfrac{\theta_a}{2\theta_s |h_m| |\ln|h_d||} \left\{ \begin{array}{l} \mathrm{e}^{L^2} \mathrm{erf}\left(P(h)+L\right) + \dfrac{h_m}{h}\left[\mathrm{erfc}(P(h))-2\right] - \\ M_1 \mathrm{e}^{L^2} \mathrm{erf}\left(P(h)+L\right) - \dfrac{2Lh_m}{h\sqrt{\pi}} \mathrm{e}^{-P^2(h)} \end{array} \right\} \right]_{h_d}^{h} }{\left[\dfrac{\theta_a}{2\theta_s |h_m| |\ln|h_d||} \left\{ \begin{array}{l} \mathrm{e}^{L^2} \mathrm{erf}\left(P(h)+L\right) + \dfrac{h_m}{h}\left[\mathrm{erfc}(P(h))-2\right] - \\ M_1 \mathrm{e}^{L^2} \mathrm{erf}\left(P(h)+L\right) - \dfrac{2Lh_m}{h\sqrt{\pi}} \mathrm{e}^{-P^2(h)} \end{array} \right\} \right]_{h_d}^{0} } \right\}^{\gamma} \\[10ex]
= K_s S_e^{\tau} \left\{ \dfrac{\begin{array}{l} \mathrm{e}^{L^2}\left[\mathrm{erf}\left(P(h)+L\right)-\mathrm{erf}\left(P(h_d)+L\right)\right] + \\ h_m\left[\dfrac{\mathrm{erfc}(P(h))-2}{h} - \dfrac{\mathrm{erfc}(P(h_d))-2}{h_d}\right] - \\ M_1\mathrm{e}^{L^2}\left[\mathrm{erf}\left(P(h)+L\right)-\mathrm{erf}\left(P(h_d)+L\right)\right] - \\ \dfrac{2Lh_m}{\sqrt{\pi}}\left(\dfrac{\mathrm{e}^{-P^2(h)}}{h}-\dfrac{\mathrm{e}^{-P^2(h_d)}}{h_d}\right) \end{array}}{\begin{array}{l} -\mathrm{e}^{L^2}\left[1+\mathrm{erf}\left(P(h_d)+L\right)\right] + \\ h_m\left[\dfrac{\mathrm{erfc}(P(0))-2}{0} - \dfrac{\mathrm{erfc}(P(h_d))-2}{h_d}\right] + \\ M_1\mathrm{e}^{L^2}\left[1+\mathrm{erf}\left(P(h_d)+L\right)\right] - \dfrac{2Lh_m}{\sqrt{\pi}}\left(\dfrac{\mathrm{e}^{-P^2(0)}}{0}-\dfrac{\mathrm{e}^{-P^2(h_d)}}{h_d}\right) \end{array}} \right\}^{\gamma}, & h_d < h \le 0
\end{cases}
$$
(18c)

where S_e is obtained by dividing Eq. (18a) by θ_s. The following functions and derived variables have been used for clarity:

410

$$
L = \frac{\sigma\sqrt{2}}{2}
$$
(18d)

$$
P(h) = \frac{\ln\left(\dfrac{h}{h_m}\right)}{\sigma\sqrt{2}}
$$
(18e)

$$M_1 = \left(1 - \frac{\theta_s}{\theta_a}\right)\ln|h_d| - \ln|h_m| + \sigma^2 \qquad (18f)$$

415

For $\kappa = 2$, the expression for the hydraulic conductivity reads:

$$K(h) = \begin{cases} 0, & h \le h_d \\[2ex] K_s S_e^\tau \left\{ \dfrac{\left[\dfrac{\theta_a}{2\theta_s h_m^2 \ln|h_d|}\left\{\dfrac{e^{4L^2}\mathrm{erf}\left(P(h)+2L\right)}{2} + \dfrac{1}{2}\left(\dfrac{h_m}{h}\right)^2\left[\mathrm{erfc}\left(P(h)\right)-2\right] - M_2 e^{4L^2}\mathrm{erf}\left(P(h)+2L\right) - \dfrac{2Lh_m^2}{h^2\sqrt{\pi}}e^{-P^2(h)}\right\}\right]_{h_d}^{h}}{\left[\dfrac{\theta_a}{2\theta_s h_m^2 \ln|h_d|}\left\{\dfrac{e^{4L^2}\mathrm{erf}\left(P(h)+2L\right)}{2} + \dfrac{1}{2}\left(\dfrac{h_m}{h}\right)^2\left[\mathrm{erfc}\left(P(h)\right)-2\right] - M_2 e^{4L^2}\mathrm{erf}\left(P(h)+2L\right) - \dfrac{2Lh_m^2}{h^2\sqrt{\pi}}e^{-P^2(h)}\right\}\right]_{h_d}^{0}} \right\}^{\gamma} \\[4ex] = K_s S_e^\tau \left\{\dfrac{\begin{aligned}&\dfrac{e^{4L^2}}{2}\left[\mathrm{erf}\left(P(h)+2L\right)-\mathrm{erf}\left(P(h_d)+2L\right)\right]+\\ &\dfrac{h_m^2}{2}\left[\dfrac{\mathrm{erfc}\left(P(h)\right)-2}{h^2} - \dfrac{\mathrm{erfc}\left(P(h_d)\right)-2}{h_d^2}\right]-\\ &M_2 e^{4L^2}\left[\mathrm{erf}\left(P(h)+2L\right)-\mathrm{erf}\left(P(h_d)+2L\right)\right]-\\ &\dfrac{2Lh_m^2}{\sqrt{\pi}}\left(\dfrac{e^{-P^2(h)}}{h^2}-\dfrac{e^{-P^2(h_d)}}{h_d^2}\right)\end{aligned}}{\begin{aligned}&-\dfrac{e^{4L^2}}{2}\left[1+\mathrm{erf}\left(P(h_d)+2L\right)\right]+\\ &\dfrac{h_m^2}{2}\left[\dfrac{\mathrm{erfc}\left(P(0)\right)-2}{0^2} - \dfrac{\mathrm{erfc}\left(P(h_d)\right)-2}{h_d^2}\right]+\\ &M_2 e^{4L^2}\left[1+\mathrm{erf}\left(P(h_d)+2L\right)\right]-\dfrac{2Lh_m^2}{\sqrt{\pi}}\left(\dfrac{e^{-P^2(0)}}{0^2}-\dfrac{e^{-P^2(h_d)}}{h_d^2}\right)\end{aligned}}\right\}^{\gamma} ,\ h_d < h \le 0 \end{cases} \qquad (18g)$$

with

420 $\qquad M_2 = \left(1 - \dfrac{\theta_s}{\theta_a}\right)\ln|h_d| - \ln|h_m| + 2\sigma^2 \qquad (18h)$

There are several terms with zero in the denominator in Eqs. (18c) and (18h). In these terms, the numerator is zero as well. The terms $\exp(P^{-2}(h)) \cdot h^{-1}$ and $\exp(P^{-2}(h)) \cdot h^{-2}$ appearing in Eqs. (18c) and (18h) both become infinite for all physically acceptable values of h_m and σ. As a consequence, the unsaturated hydraulic conductivity for both values of κ suffers from the non-realistic increase near saturation diagnosed by Ippisch et al. (2006) for van Genuchten's (1980) soil water retention model, and the use of Eqs. (18c-h) is not recommended.

Groenevelt and Grant (2004) proposed:

$$\theta(h) = \begin{cases} 0, & h \leq -10^{6.9}\,\text{cm} \\ g_1\left\{\exp\left(\dfrac{-g_0}{6.9^\eta}\right) - \exp\left[\dfrac{-g_0}{\left(\log_{10}|h|\right)^\eta}\right]\right\}, & -10^{6.9} \leq h \leq -1\,\text{cm} \\ g_1\exp\left(\dfrac{-g_0}{6.9^\eta}\right), & h \geq -1\,\text{cm} \end{cases} \tag{19a}$$

where g_0, g_1, and η are fitting parameters. The constant water content for matric potentials larger than -1cm is imposed. Groenevelt and Grant (2004) proposed a more flexible curve-shifting approach, but that procedure is cumbersome to perform in a global search parameter fitting operation. The derivative is

$$\frac{\mathrm{d}\theta}{\mathrm{d}h} = \begin{cases} 0, & h \leq -10^{6.9}\,\text{cm} \\ \dfrac{g_0 g_1 \eta [\ln(10)]^\eta}{|h|(\ln|h|)^{\eta+1}} \exp\left\{\dfrac{-g_0[\ln(10)]^\eta}{(\ln|h|)^\eta}\right\}, & -10^{6.9} \leq h \leq -1\,\text{cm} \\ 0, & h \geq -1\,\text{cm} \end{cases} \tag{19b}$$

This expression does not permit a closed-form expression for the hydraulic conductivity function.

Peters (2013) introduced four soil water retention models. He used a logarithmic model for adsorbed water that differed from that of Campbell and Shiozawa (1992) and the capillary model of either van Genuchten (1980) or Kosugi (1999). He developed versions for which the water content could be non-zero at the oven-dry matric potential h_d, which is incorrect but permits closed-from expressions of the hydraulic conductivity function. He also presented versions for which the water content is forced to be zero at h_d.

For the versions with nonzero water contents at h_d, the capillary bound and adsorbed water contents are added (Peters, 2013, Eq. (2))

$$S_e(h) = wS^{cap}(h) + (1-w)S^{ad}(h) \tag{20}$$

where the superscripts cap, and ad reflect capillary bound and adsorbed water, respectively, and w is a weighting factor ranging between 0 and 1. The van Genuchten-version with non-zero water content at h_d is

450

$$\theta(h) = \begin{cases} \theta_s w\left[1 + \left(-\alpha h\right)^n\right]^{\frac{1}{n}-1} + \theta_s(1-w)\dfrac{1 - \dfrac{\ln\left(1 + \dfrac{h}{h_a}\right)}{\ln\left(1 + \dfrac{h_d}{h_a}\right)}}{1 - \dfrac{\ln(2)}{\ln\left(1 + \dfrac{h_d}{h_a}\right)}}, & h_d \le h \le h_a \\[2em] \theta_s w\left[1 + \left(-\alpha h\right)^n\right]^{\frac{1}{n}-1} + \theta_s(1-w), & 0 \ge h \ge h_a \end{cases}$$

(21a)

with derivative

$$\dfrac{d\theta}{dh} = \begin{cases} -\theta_s w\alpha(1-n)\left(-\alpha h\right)^{n-1}\left[1 + \left(-\alpha h\right)^n\right]^{\frac{1}{n}-2} + \dfrac{\theta_s(1-w)}{h + h_a}\dfrac{1}{\ln\left(1 + \dfrac{h_d}{h_a}\right) - \ln(2)}, & h \le h_a \\[2em] -\theta_s w\alpha(1-n)\left(-\alpha h\right)^{n-1}\left[1 + \left(-\alpha h\right)^n\right]^{\frac{1}{n}-2}, & 0 \ge h \ge h_a \end{cases}$$

(21b)

455

The parameter h_a [L] represents the matric potential at which the soil reaches the maximum adsorbed water content.

The Kosugi-version with non-zero water content at air-dryness is

$$\theta(h) = \begin{cases} \dfrac{\theta_s w}{2}\,\text{erfc}\left[\dfrac{\ln\left(\dfrac{h}{h_m}\right)}{\sigma\sqrt{2}}\right] + \theta_s(1-w)\dfrac{1 - \dfrac{\ln\left(1 + \dfrac{h}{h_a}\right)}{\ln\left(1 + \dfrac{h_d}{h_a}\right)}}{1 - \dfrac{\ln(2)}{\ln\left(1 + \dfrac{h_d}{h_a}\right)}}, & h_d \le h \le h_a \\[3em] \dfrac{\theta_s w}{2}\,\text{erfc}\left[\dfrac{\ln\left(\dfrac{h}{h_m}\right)}{\sigma\sqrt{2}}\right] + \theta_s(1-w), & 0 \ge h \ge h_a \end{cases}$$

(22a)

460

with derivative

$$\frac{d\theta}{dh} = \begin{cases} -\dfrac{\theta_s w}{h\sigma\sqrt{2\pi}}\exp\left\{-\left[\dfrac{\ln\left(\dfrac{h}{h_m}\right)}{\sigma\sqrt{2}}\right]^2\right\} + \dfrac{\theta_s(1-w)}{h+h_a}\dfrac{1}{\ln\left(1+\dfrac{h_d}{h_a}\right)-\ln(2)}, & h \le h_a \\[2em] -\dfrac{\theta_s w}{h\sigma\sqrt{2\pi}}\exp\left\{-\left[\dfrac{\ln\left(\dfrac{h}{h_m}\right)}{\sigma\sqrt{2}}\right]^2\right\}, & 0 \ge h \ge h_a \end{cases} \tag{22b}$$

465   The van Genuchten-version with zero water content when the soil is air dry is

$$\theta(h) = \begin{cases} 0, & h \le h_d \\[1em] \theta_s\left(w\left\{\left[1+(-\alpha h)^n\right]^{\frac{1}{n}-1}-1\right\}+1\right)\dfrac{1-\dfrac{\ln\left(1+\dfrac{h}{h_a}\right)}{\ln\left(1+\dfrac{h_d}{h_a}\right)}}{1-\dfrac{\ln(2)}{\ln\left(1+\dfrac{h_d}{h_a}\right)}}, & h_d \le h \le h_a \\[2em] \theta_s w\left[1+(-\alpha h)^n\right]^{\frac{1}{n}-1}+\theta_s(1-w), & 0 \ge h \ge h_a \end{cases} \tag{23a}$$

with derivative

470

$$\frac{\mathrm{d}\theta}{\mathrm{d}h} = \begin{cases} 0, & h \le h_d \\[2em] -\theta_s w \alpha (1-n)(-\alpha h)^{n-1}\left[1+(-\alpha h)^n\right]^{\frac{1}{n}-2} \dfrac{1 - \dfrac{\ln\left(1+\dfrac{h}{h_a}\right)}{\ln\left(1+\dfrac{h_d}{h_a}\right)}}{1 - \dfrac{\ln(2)}{\ln\left(1+\dfrac{h_d}{h_a}\right)}} & \\[3em] +\dfrac{\theta_s\left(w\left\{\left[1+(-\alpha h)^n\right]^{\frac{1}{n}-1}-1\right\}+1\right)}{(h+h_a)\left[\ln\left(1+\dfrac{h_d}{h_a}\right)-\ln(2)\right]}, & h \le h_a \\[2em] -\theta_s w \alpha (1-n)(-\alpha h)^{n-1}\left[1+(-\alpha h)^n\right]^{\frac{1}{n}-2}, & 0 \ge h \ge h_a \end{cases} \qquad (23b)$$

The Kosugi-version with zero water content at h_d is

$$475 \quad \theta(h) = \begin{cases} 0, & h \le h_d \\[2em] \theta_s\left(w\left\{\frac{1}{2}\mathrm{erfc}\left[\dfrac{\ln\left(\dfrac{h}{h_m}\right)}{\sigma\sqrt{2}}\right]-1\right\}+1\right)\dfrac{1 - \dfrac{\ln\left(1+\dfrac{h}{h_a}\right)}{\ln\left(1+\dfrac{h_d}{h_a}\right)}}{1 - \dfrac{\ln(2)}{\ln\left(1+\dfrac{h_d}{h_a}\right)}}, & h_d \le h \le h_a \\[3em] \dfrac{\theta_s w}{2}\mathrm{erfc}\left[\dfrac{\ln\left(\dfrac{h}{h_m}\right)}{\sigma\sqrt{2}}\right]+\theta_s(1-w), & 0 \ge h \ge h_a \end{cases} \qquad (24a)$$

with derivative

$$
\frac{\mathrm{d}\theta}{\mathrm{d}h} = \begin{cases}
0, & h \le h_d \\[2em]
-\dfrac{\theta_s w}{h\sigma\sqrt{2\pi}} \exp\left\{-\left[\dfrac{\ln\left(\dfrac{h}{h_m}\right)}{\sigma\sqrt{2}}\right]^2\right\} \dfrac{1 - \dfrac{\ln\left(1+\dfrac{h}{h_a}\right)}{\ln\left(1+\dfrac{h_d}{h_a}\right)}}{1 - \dfrac{\ln(2)}{\ln\left(1+\dfrac{h_d}{h_a}\right)}} & \\[2em]
+\left(w\left\{\dfrac{1}{2}\operatorname{erfc}\left[\dfrac{\ln\left(\dfrac{h}{h_m}\right)}{\sigma\sqrt{2}}\right]-1\right\}+1\right)\dfrac{\theta_s}{(h+h_a)\left[\ln\left(1+\dfrac{h_d}{h_a}\right)-\ln(2)\right]}, & h \le h_a \\[2em]
-\dfrac{\theta_s w}{h\sigma\sqrt{2\pi}} \exp\left\{-\left[\dfrac{\ln\left(\dfrac{h}{h_m}\right)}{\sigma\sqrt{2}}\right]^2\right\}\Bigg\}, & 0 \ge h \ge h_a
\end{cases}
\tag{24b}
$$

480

Both water retention functions based on van Genuchten's (1980) model (Eqs. (21a) and (23a)) lead to the requirement that κ be smaller than n-1 (see Eq. (9)) and therefore do only have a physically acceptable conductivity curve associated with them for a very limited range of κ. The Kosugi-based versions (Eqs. (22a) and (24a)) suffer from the same lack of clarity about the behavior of the derivative as Khlosi et al.'s (2008) modified Kosugi function and require integer values of κ. Because of these limitations and the unwieldy nature of the equations (compare Eqs. (18c-h)), their practical value seems limited.

Iden and Durner (2014) proposed modifications of Peters' (2013) models that permitted an analytical expression for the conductivity function even if the water content was forced to be zero at h_d. To apply the criterion of Eq. (4) to this modification, we multiply the derivative of their retention curve (their Eq. (3)) for adsorbed water by $h^{-\kappa}$:

$$
\theta_s |h|^{-\kappa}\frac{\mathrm{d}S^{ad}}{\mathrm{d}h} = \frac{\theta_s |h|^{-\kappa-1}}{\ln(10)\big(\log|h_a|-\log|h_d|\big)}\left[1-\frac{\exp\left(\dfrac{\log|h_a|-\log|h|}{b}\right)}{1+\exp\left(\dfrac{\log|h_a|-\log|h|}{b}\right)}\right]
\tag{25}
$$

where *b* is a shape parameter. High values of *b* lead to a sharp transition between the two linear segments in the semi-logarithmic form of the adsorbed water retention curve with different slopes. Iden and Durner recommend values of *b* between 0.1 and 0.3.

In the limit as *h* approaches zero, Eq. (25) simplifies to

$$\lim_{h \to 0}\left(\theta_s |h|^{-\kappa}\frac{dS^{ad}}{dh} \right) = \frac{\theta_s |h|^{-\kappa-1}}{\ln(10)(\log|h_a| - \log|h_d|)}\left[1 - \frac{\exp\left(\dfrac{-\log|h|}{b}\right)}{1 + \exp\left(\dfrac{-\log|h|}{b}\right)} \right] \tag{26}$$

The approximation in the last term leads to the requirement that $\kappa < -1$ for the limit to go to zero for any value of *b*, but small values of *b* allow larger ranges of κ. For $b = 0.3$, trial calculations showed that the value in the limit appears to be zero for $\kappa < 0.2$, which still rules out the established conductivity models. For $b = 0.1$, the limit is zero even for large positive values of κ. It might be recommendable to fix *b* at 0.1 instead of treating it as a fitting parameter.

The scaling of the capillary soil water retention curves proposed by Iden and Durner (2014) does not alleviate the problems with the van Genuchten curve near saturation while the Kosugi-function remains unwieldy. Conductivity functions for Peters' (2013) retention models will therefore not be derived.

In summary, many of the retention curves examined result in conductivity curves with physically unacceptable behavior near saturation, even though several of these expressions were derived with the explicit purpose of providing closed-form expressions for the hydraulic conductivity. Only the Brooks-Corey function (1964) (BCO, Eq. (5a)), the junction model of Rossi and Nimmo (1994) without the parabolic correction (RNA, Eq. (13a)), and the model of Fayer and Simmons (1995) based on the Brooks-Corey (1964) retention function (FSB, Eq. (16a)) lead to an acceptable conductivity model with full flexibility (three free parameters: κ, γ, τ). The modified van Genuchten (1980) retention curve with a distinct air-entry value by Ippisch et al. (2006) (VGA, Eq. (11a)) leads to a conductivity model with two fitting parameters if $m = 1 - 1/n$ because $\kappa = 1$.

3. Materials and methods

3.1. Soil water retention and hydraulic conductivity data

Data were obtained from Schelle et al. (2013) who measured soil water retention curves for a range of soil textures (clay, silt, silt loam, and sand). The retention data were measured on soil samples using different laboratory methods and cover the moisture range from saturation to near oven dryness at pF approximately 7. For details on the measurement methods we refer to Schelle et al. (2013).

For silt, silt loam and sand we used data obtained by suction plates (used with 4.0 cm high samples), pressure plates and the dew point method (drying). To obtain an even distribution of measurements over the whole

moisture range, data obtained by the evaporation method (HYPROP®), which produces a large number of measurements within its relatively wet measurement range, were excluded.

530 For clay we used HYPROP (until pF 3), pressure plate and drying dew point methods but trimmed the data set in the HYPROP range by stratifying the data into intervals of 0.5 on the pF scale and then randomly picking one data point for each interval. This ensured an adequate sensitivity of the fit in the dry range for all textures. For some of the soil samples, hydraulic conductivity data were available, including the values at saturation (unpublished). Hydraulic conductivity data were obtained by the evaporation method according to Peters and Durner (2008).

535 The fitting routine uses the variance of the data error to determine the weighting factor each data point. We estimated these on the basis of estimated measurement errors of water level readings, pressure gauges, sample masses, etc.

When the three conductivity parameters are set to the values dictated by Burdine (1953), Mualem (1976), or Alexander and Skaggs (1986), hydraulic conductivity curves can be derived from soil water retention data only, supplemented by an estimate for the saturated hydraulic conductivity. For the soils with available conductivity data

540 we compared the hydraulic conductivity curves to the direct measurements.

3.2. Parameter fitting
3.2.1. Selected parameterizations

545 We fitted the parameterizations that gave physically plausible near-saturated hydraulic conductivity behavior: BCO, FSB, RNA (all three conductivity models), and VGA (only Burdine's (1953) and Mualem's (1976) conductivity models). For comparison we also fitted VGN (only Mualem's, conductivity model) as it is the most widely used parameterization at the moment. Table 1 shows the fitting parameters and their physically permitted range.

550 ### 3.2.2. The objective function and its weighting factors

A set of parameters describing the soil water retention curve must be optimized to provide the best fit to an arbitrary number of data points. To do so, an objective function was minimized, construed by the sum of weighted squares of the differences between observed and fitted values. The fitted values depend on the parameter values in

555 the parameter vector $\mathbf{x}$. Assume q_θ observation pairs of water content vs. matric head (h_i, θ_i). Here, θ_i denotes the ith observation of the volumetric water content, h_i [L] is the matric head at which that water content was observed (expressed as an equivalent water column), and $i \in \{1,2,\ldots, q_\theta\}$ is a counter. In the code, the assumed units are cm water column for h and cm^3 cm^{-3} for θ.

The definition of the objective function $F_R(\mathbf{x}_{p,R})$ at the Rth iteration during the fitting operation is:

560

$$F_R(\mathbf{x}_{p,R}) = \mathbf{w}_{\theta,R}^{\mathrm{T}} \mathbf{d}_\theta(\mathbf{x}_{p,R}, \mathbf{x}_f) \quad R \in \{1,2,\ldots,R_{\max}\} \tag{27}$$

Here, $\mathbf{d}_\theta$ denotes a vector of length q_θ of squared differences between observations and fits that are functions of the fitted parameter values $\mathbf{x}_p$ and the fixed (non-fitted) parameters in vector $\mathbf{x}_f$. Together, $\mathbf{x}_p$ and $\mathbf{x}_f$ constitute $\mathbf{x}$. Each

565   squared difference is weighted. The weight factor vector is denoted by $\mathbf{w}_{\theta,R}$. Its dependence on the water content and iteration step is explained below. The superscript T indicates that the vector is transposed. To terminate infinite loops, the number of iterations is capped by $R_{\max}$.

For relatively wet soils ($0 > h > $ -100 to -200 cm), measurement methods are available that create a hydrostatic equilibrium in a relatively large sample. In such cases h_i reflects the matric potential at the center of the

570   sample but θ_i is that determined for the entire sample. The vertical variation of h results in a non-uniform water content, and the average water content of the sample (θ_i) may not be well represented by the water content corresponding to h_i. For these cases, the height of the sample can be specified on input. The code then divides the sample into 20 layers, calculates h in the center of each layer, computes the corresponding water contents from $\mathbf{x}_{p,R}$, and averages these to arrive at an estimate of θ_i.

575   If and only if the standard deviation of the measurement error of the individual observations is known, a maximum-likelihood estimate of the soil hydraulic parameters can be obtained (Hollenbeck and Jensen, 1998). To ensure this, the weighting factors in vector $\mathbf{w}_{\theta,R}$ must be equal to the reciprocal of the variance of the measurement error. Note that this choice eliminates any effect of measurement units because the squared differences have the same units as the variances by which they are divided (Hollenbeck and Jensen, 1998). Only then can model

580   adequacy be examined. A model is considered adequate if the residuals after parameter fitting are solely caused by measurement noise (Hollenbeck et al., 2000). Furthermore, only if these conditions are met can confidence intervals of fitted parameters be determined (Hollenbeck and Jensen, 1998). Even in that case, the contouring of the parameter space for permissible increases of the objective function required to determine the confidence region is not practically feasible for four or more parameters, and very laborious even for fewer parameters. A popular

585   approximation based on the Cramer-Rao theorem was shown to be rather poor by Hollenbeck and Jensen (1998), so we refrained from implementing it. Instead we record the evolution of the parameter values through the iterative process. Low information content (indicated by large random fluctuations of a parameter value), correlated parameters, and parameters trending towards a minimum or maximum permitted value can usually be diagnosed from such records.

590   Data points for a retention curve over the whole moisture range cannot be obtained by a single method. Furthermore, measurement errors occur in both h_i and θ_i. To accommodate this, the error standard deviations $\sigma_{h,i}$ and $\sigma_{\theta,i}$ for h and θ, respectively can be provided individually for any data point i. To improve the performance of the fitting routine, the values of $\sigma_{\theta,i}$ are scaled to ensure their average equals 0.20, i.e., the same order of magnitude as θ. The values of $\sigma_{h,i}$ are then scaled by the same scaling factor. The weighting factor $w_{R,i}$ for observation θ_i during

595   iteration R is:

$$w_{R,i} = \sigma^{*\,-2}_{i,R} = \left(\sigma^{*}_{h,i} \left. \frac{\mathrm{d}\theta}{\mathrm{d}h} \right|_{R,i} + \sigma^{*}_{\theta,i} \right)^{-2} \tag{28}$$

where the asterisk denotes a scaled value. The subscripts i and R label data points and iteration steps as above. The
600 gradient is determined from the Rth fitted $\theta(h)$ relationship defined by $\mathbf{x}_{p,R}$. Thus, the weighting factors are updated
for every iteration.

In the code, the gradient is approximated by $\Delta\theta/\Delta h$ computed from the water contents at $h_i \pm \max(1$ cm
H_2O, $0.01 \cdot h_i)$. For data points acquired at hydrostatic equilibrium, this would require 40 additional calls to the
function that computes the θ corresponding to a given value of h, which would be rather inefficient. Instead, the
605 water content is calculated for one virtual layer below and one above the sample. By subtracting the water content of
the top (bottom) layer in the sample and adding the water content of the virtual layer below (above) the sample, the
water content corresponding to $h_i + H/20$ ($h_i - H/20$) can be found, with H the sample height in cm. In this way,
$\Delta\theta/\Delta h$ can be computed with only two additional calls to the function that defines the parameterized $\theta(h)$
relationship.

610

3.2.3. Parameter optimization by Shuffled Complex Evolution

The calibration algorithm employed here is the Shuffled Complex Evolution (SCE) algorithm introduced by
Duan et al. (1992) with parameter adjustments of Behrangi et al. (2008). The strategy of this algorithm is to form out
of $j + 1$ parameter sets, where j is the number of model parameters, so-called complexes (e.g. triangles in 2D). Each
615 vertex of the complex not only represents one of the $j + 1$ parameter sets but also the model's skill $F_R(\mathbf{x}_{p,R})$ to match
the observed data when it is forced with the according parameter set $\mathbf{x}_{p,R}$. This skill is usually referred to be the
objective function value of an objective to be minimized. The vertex with the worst skill or largest objective
function value is subsequently perturbed in order to find a better substitute parameter set. This strategy is repeated
until the volume of the complex, i.e. the agreement of the parameter sets, is smaller than a threshold. To avoid that
620 the search gets stuck in a local optimum, a number of Y complexes are acting in parallel. After a certain number of
iterations the $Y \cdot (j + 1)$ vertexes are shuffled and newly assigned to Y complexes. The algorithm converges when the
volume of all complexes is lower than a threshold which means that all $Y \cdot (j + 1)$ vertexes are in close proximity to
each other. Infinite runs of the SCE are avoided by $R_{\max}$, but convergence should be the desired target for
termination of the SCE.

625 The SCE algorithm used here is configured with two complexes each consisting of $(2j + 1)$ ensemble
members. The different parameterizations we fitted had 3 to 5 fitting parameters. In each iteration $j + 1$ parameters
are randomly selected and the vertex with the worst skill is perturbed. The reflection and contraction step lengths in
the Simplex method (e.g., Press et al., 1992, p. 402-404) were set to 0.8 and 0.45, respectively. SCE seems to have
an order of about $\mathrm{O}(j^2)$. In our case it required between 280 and 1735 model evaluations to find the optimal
630 parameter set. For each parameter estimation run, three sets of initial guesses of the fitting parameters must be
provided. The results of the three trials were compared to reduce the chance of accepting a local minimum of the
objective function. The selection of SCE was based on its widespread usage in hydrological studies and according to
a preliminary experiment where the SCE outperformed other algorithms like the Simulated Annealing (Kirkpatrick
et al, 1983) and the Dynamically Dimensioned Search algorithm (Tolson et al., 2007) in optimizing more than 80
635 analytical test functions with j ranging from 2 to 30.

3.3. Scenario study by numerical simulations

As stated in the Introduction, previous tests of parametric expressions of soil water retention functions mostly focused on the quality of the fit to direct observations of points on the water retention curve. Here, we will also examine how the various parameterizations affect the solution of Richards' equation by simulating water fluxes and soil water profiles for a scenario involving infiltration and evaporation. We set up a hypothetical 999-day scenario representative of a desert climate with prolonged drying, infiltration into dry soil, and redistribution after rainfall, permitting a comprehensive test of the parameterizations. We used the HYDRUS 1-D model version 4.xx (Šimůnek et al., 2013, http://www.pc-progress.com/en/Default.aspx?hydrus-1d) to solve Richards' equation in a 1-dimensional soil profile. We permitted flow of liquid water as well as diffusive water vapor fluxes.

We considered an unvegetated uniform soil profile of 1 m depth, initially in hydrostatic equilibrium with -400 cm matric potential at the soil surface. The upper boundary conditions were atmospheric (during dry periods: prescribed matric potential set to -50000 cm; during rain: prescribed flux density equal to the daily rainfall rate derived from observed daily sums). At the bottom of the profile, free drainage was assumed. The weather data (daily rainfall and temperature) were taken from the NOAA data base (http://www.ncdc.noaa.gov/cdo-web/) for a station in Riyadh city (Saudi Arabia) between June 4, 1993 and February 27, 1996. In this period spanning nearly three years, there were three clusters of rainfall events Fig. 1. The second cluster was the heaviest with a maximum daily sum of approximately 5.4 cm at the day 656.

The various parameterizations are not implemented in HYDRUS. We therefore used the MATER.IN input file to supply the soil hydraulic property curves in tabular form to the model. The retention models BCO, FSB, and RNA permitted all three conductivity models (Burdine, Mualem and Alexander and Skaggs) to be used. VGA only gives useful expressions for Burdine and Mualem. VGN only allows Mualem's conductivity model. Thus, there are 12 combinations of retention and conductivity curves that we tested on four different textures, leading to 48 different simulations (and MATER.IN files) in total.

4. Results and discussion

4.1 Fitted parameters and quality of the fits

Table 1 presents the fitted parameters for all combinations of texture and parameterization. The parameter with the best-defined physical meaning is θ_s. All parameterizations give comparable values for it for each texture, which reflects the relatively narrow data clouds near saturation. The values of θ_r are relatively high for the three parameterizations in which it occurs. The air-entry values (h_{ae}) should increase (move closer to zero) from clay to silt loam to silt to sand, which is the case for BCO, FSB, and RNA, but not for VGA. The data in Fig. 2 support relatively similar values for all textures other than clay, which is somewhat surprising. RNA gives rather high values in silt and sand, and VGA does very poorly in sand and silt loam. The high value for h_{ae} for FSB in clay may be related somehow to the very high value of the maximum adsorbed water content θ_a, which we fixed close to θ_s. The value of θ_a for clay should be larger than that for silt loam, so it cannot be more than about 0.2 off though. The spread of h_j for RNA across the textures show that this parameter needs to be given the full range (between h_d and at

least the minimum value of h_{ae}). Even with initial guesses that differed by several orders of magnitude, the fits were
675 still quite consistent, so evidently these values are supported by the data and not an artefact.

In three of the 48 parameter estimation runs, the fits pushed one of the parameters to one of its bounds (even after expanding these to their physical limits), irrespective of their initial guess: FSB for clay (we fixed θ_a to 0.5), VGN for sand and RNA for silt (we fixed θ_s on the basis of the data in both cases). For BCO and VGA in sandy soil, the code could not converge to a global minimum, indicated by the volume of the complexes, which
680 exceeded the threshold. The fitted parameters should be viewed critically in these two cases.

The Root Mean Square Error (RMSE) of the fits (Table 2) illustrate why VGN has been very popular for over three decades. It gives the best fit in three cases (sand, silt and silt loam) and the second-best fit in the fourth (clay). BCO performs poorest in three cases (sand, silt and silt loam) and second-poorest in one (clay). The other three have varying positions, with no clearly strong or weak performers. FSB has the best performance in the finest
685 soil (clay). The overall difference in the RMSE values between textures reflects the different scatter in the underlying data clouds.

The soil water retention curves defined by the different pits are plotted in (Fig. 2). The models that were not developed with dry conditions in mind (BCO, VGA and VGN) have relatively high water contents in the dry end of clay and silt loam. The logarithmic dry end of FSB and RNA eliminates this asymptotic behavior. The cutoff to zero
690 of the FSB parameterization is quite strong in fine-textured soils. The fixed value of h_d (where the water content is zero) of RNA seems to be too small for clay while appearing adequate for the other textures.

In the intermediate range, all fits are close to one another. RNA underperforms in sand and silt compared to the others. In the wet range, the absence of an air-entry value in VGN results in a poor fit for sand. Here, the contrast between VGN and VGA is very clear. Overall, the inclusion of the water-entry value as a parameter seems
695 beneficial to the fits. FSB has the most satisfactory overall performance.

For sand, silt, and silt loam, independent observations of $K(h)$ were available. The fits of Burdine's (1953) and Mualem's (1976) parameterizations based on retention data only were remarkably good for all parameterizations. The function of Alexander and Skaggs (1986) severely overestimated the hydraulic conductivity in all three cases, but very accurately described the slope of the curve for silt loam. Fig.3 demonstrates this for FSB,
700 the results for the other parameterizations were comparable.

4.2. Simulation results
4.2.1 Silt

705 We start the analysis by examining the flux at the bottom of the soil profile. Panels a-e of (Fig. 4) show all combinations of parameterizations of the retention and conductivity curves.

The early rainfall cluster event at around $t = 300$ d did not generate any bottom flux, and therefore only wetted up the soil profile. In doing so it increased the effect of the heavier rainfall around $t = 656$ d on the bottom flux.

710   For the individual parameterizations, Mualem (M) and Burdine (B) gave reasonably similar results in which the second and third rainfall cluster generated a little more downward flow for B than for M. In all cases, Alexander and Skaggs (AS) gave a more rapid response of a very different magnitude. Clearly visible is a sustained, constant flux leaving the column during prolonged dry periods for the AS conductivity curves. This is physically implausible.

Fig. 4f shows the substantial effect of the parameterization of the water retention curve on bottom fluxes
715   when the M-type $K(h)$ function is deployed. The results for B-type $K(h)$ were comparable. Different retention curves gave very different responses to the initial conditions, highlighting the need to add a sufficiently long lead time ahead of the target time window to the simulated time period. RNA's response to the second and third rainfall clusters was about 2.4 times that of the others. At h = -300 cm (pF 2.48), K according to M is at least 5 times higer for RNA than for the rest, while the water content at that matric potential and higher values is relatively small (Fig.
720   2c). Thus, infiltrated water was transported downward with relative ease, giving rise to the relatively high bottom fluxes and low evaporation rates that were computed for RNA (Figs. 4f, 5f).

If the remarkable response of VGA to the initial condition compared to VGN is disregarded, the parameterizations other than RNA behaved rather similar, except for the fact that VGA responded much faster to a change in the forcings than the other parameterizations. VGN's response to the initial condition and to rainfall was
725   more tailed than that of the other parameterizations.

Fig. 4g shows the similar comparison of all parameterizations for the AS-type $K(h)$ function. The response to rainfall was very fast and short-lived, which seems improbable for a silt soil that is far from full saturation. The non-physical bottomflux during dry periods (especially for VGA), the slow calculation times (half as fast as the others) with the time step always at the smallest permitted value, and non-negligible mass balance errors all point to
730   numerical problems associated with AS.

The evaporative flux was nearly identical for B and M conductivity functions (Fig. 5a-c). Since their bottom fluxes differed, this necessarily implies that the storage in the soil profile must also be different for B and M. The AS parameterization gave a much more spiky response of evaporative flux to rainfall than B or M, with zero evaporation most of the time (Fig. 5a-d). In terms of cumulative evaporation, AS responded more strongly to the
735   initial condition (Fig. 5a-c) and, to a lesser degree, to the second rainfall cluster around t = 650 d. Overall, the effect of the conductivity function on evaporation was less pronounced than on the bottom flux, and was dominated by the response to the initial condition. The same was true for the parameterization of the retention curve, as demonstrated by the relatively similar shapes of the curves in panels f and g of Fig. 5. Strikingly, the correction of Ippish et al. 2006, which created the difference between VGN and VGA caused a very fast attenuation of the effect of the initial
740   conditions for the bottom flux as well as the evaporation (compare Figs. 4d and e, and Figs 5d and e).

Given the non-physical behavior of the bottom flux of AS for VGA in particular (Fig. 4d), we also examined the infiltration. We first compare infiltration for VGA with M and AS-type conductivity (Fig. 6a), and clearly see the zero infiltration for VGA during periods without rain contrasted to the impossible non-zero infiltration rates for AS during dry spells. For the other water retention parameterizations in combination with AS,
745   the effect is less pronounced (Fig. 6b). Still, the AS conductivity should be used with care and the results and mass balance checked.

Table 3 summarizes the bottom and evaporative fluxes with the effect of the initial condition removed. For evaporation, the differences are inconsequential except for the markedly low values for RNA. For the bottom flux, the difference between B and M is small enough to be within the margin of error for typical applications. The effect of the parameterization of the retention curve is an order of magnitude between the smallest bottom flux (for VGA) and the largest (for RNA).

4.2.2. Sand

The relationship between the bottom (Fig. 7) and evaporative fluxes (Fig. 8) as generated by the various parameterizations for the sandy soil were comparable to those for silt, and the analysis applied to the silt carries over to sand. The response to the initial conditions was less pronounced for AS conductivity functions, but still quite large. The bottom fluxes in sand responded faster and with less tailing than in silt, and the third rainfall cluster near the end of the simulation period produced a clear signal (Fig. 7).

Notably, the responses of the bottom fluxes to the initial conditions were much smaller in sand than they were in silt, probably because the volumetric water content in sand at a matric potential of -300 cm (at the bottom of the soil column) and -400 cm (at the top) was already well below 0.1 for all parameterizations (Fig. 2b).

The FSB (Fig. 7b) and RNA (Fig.7a) parameterizations were both in their logarithmic dry range when bottom fluxes occurred, and gave comparable values. BCO is not well adapted for dry conditions, and this is reflected by a bottom flux that is four times lower than the others (Fig 7g).

The bottom fluxes for BCO and FSB with AS-type $K(h)$ are similar (Fig.7h), in stark contrast to the bottom fluxes based on B (Fig.7f) and M (Fig.7g) for these parameterizations. The similarity in the fluxes for AS reflect the facts that the evaporative fluxes (occurring in the wet range, where BCO and FSB both have Brooks-Corey retention curves) are very similar and the spiky response typical for AS results in small difference in storage between BCO and FSB. Consequently, the bottom flux, as the only remaining term of the water balance, cannot differ strongly between BCO and FSB.

The difference in the bottom fluxes generated for VGN and VGA with M-type $K(h)$ (Fig.7g) is even more extreme than in case of the silty soil. Here too, the effect of the initial conditions lingers for a long time for VGN, even though the magnitude of the effect is smaller.

For both M and B conductivity functions, the evaporation (Figs. 8b and c) and the bottom flux (Figs.7a, f, and g) for BCO differed from the other parameterizations. These differences seem to have been dominated by the complementary responses of evaporation and bottom fluxes to the rainfall events around $t = 656$ d. BCO converted roughly 5-7 cm more of this rainfall to evaporation than the other parameterizations, for both B and M. Therefore, less water was available for downward flow, resulting in a cumulative bottom flux for BCO that was roughly 6 to 8 cm smaller than for the other parameterizations.

The AS-type $K(h)$ function again gave a spiky response (Fig. 8a). Nevertheless, the differences in the evaporation and the bottom flux compared to those of B and M are not very large. The bottom fluxes resulting from rainfall events were considerably smaller for RNA than for the other parameterizations.

785 Coarse-textured soils have the sharpest drop in the hydraulic conductivity as the soil desaturates. We therefore used the result for the sandy column to study the relationship between the matric potential at the bottom of the column and the bottom flux in order to evaluate water fluxes in dry soils. The free drainage lower boundary condition ensures there is always a downward flux that is equal to the hydraulic conductivity at the bottom at any time. Particularly for coarse soils this can still lead to negligible bottom fluxes for considerable periods of time. We first consider FSB and RNA, these being the parameterizations specifically developed to perform well in dry soils.

790 The difference in matric potentials between FSB and RNA is immediately clear from Figs. 9a, b and 10a, b. The effect of the conductivity function is manifest by including Figs. 9c and 10c in the comparison. The effect of the first rainfall cluster is visible in the matric potential in all cases (Figs. 9 and 10), but not enough to generate a significant flux. A flux through the lower boundary first occurs when the matric potential there exceeds (i.e. becomes less negative than) -70 cm for FSB (Fig. 9a and b) and -30 cm for RNA (Figs. 10a and b).

795 The second rainfall cluster at $600 < t < 700$ d did not rely on prewetting: it produced a bottom flux no matter how dry the soil was. The third rainfall cluster around day 930 probably would not have generated a bottom flux for B- and M-type $K(h)$ functions, had the previous rainfall cluster not prewetted the soil. Note that the previous rainfall affects matric potentials at 1 m depth for several hundreds of days for B and M-type conductivity functions, but only for a few months at most for AS.

800 The AS-type $K(h)$ function gave such rapid responses that only the second flux event at about 694 d was a result of recent pre-wetting at $t \approx 656$ d (Figs. 9c and 10c). Despite the very different matric potentials at the bottom, the cumulative bottom fluxes produced by a single rainfall cluster generated by FSB and RNA were quite similar for B and M and only somewhat larger for AS (Figs. 9 and 10).

The AS conductivity function led the soil to dry out so completely that the atmospheric matric potential during dry spells was reached at 1 m depth in a few months (Figs. 9c and 10c). This seems unrealistic, and seems to 805 be related to the significant overestimation of the unsaturated hydraulic conductivity by AS evidenced in Fig. 3.

For comparison, the bottom matric potentials and fluxes are given for BCO as well (Fig. 11). They are very different, and given the poor suitability of BCO for dry soils and the poor fitting performance probably incorrect. The differences between the parameterizations illustrate the need to carefully consider the suitability of the 810 parameterization for the intended purpose.

4.2.3. Silt loam and clay

The bottom fluxes from the clay and the silt loam soil for all combinations of parameterizations for the soil 815 water retention and hydraulic conductivity curves were similar to those for the silt soil (Figs. 12 and 15), with two notable exceptions: for RNA, there was a much more damped response to the rainfall around $t = 656$ d for either the B or the M-type $K(h)$ function (Fig. 12c), in comparison to the rapidly increasing bottom flux in silt. In clay, there was virtually no response anymore (Fig. 15c). In general, the bottom fluxes for all parameterizations displayed comparable behavior with the exception of those with AS-type $K(h)$ functions, which showed very strong responses 820 to the initial conditions (Figs. 12 and 15).

The behavior of the evaporative fluxes from the silt loam and the clay soil for all combinations of parameterizations for the soil water retention and hydraulic conductivity curves was essentially similar to that for the silty soil (Figs. 13 and 16). The main difference was the less gradual response of the evaporation for VGA, particularly for clay, which was, in fact, rather similar to the notoriously spiked response of the AS-type

825   conductivity function. The relative amounts of evaporation of the various parameterizations varied from one texture to another.

For AS in combination with the VGA retention curve, there was significant infiltration during periods of zero rainfall (Figs. 14 and 17). This numerical artefact led to erroneous simulations of the bottom flux. This is the most significant occurrence of mass balance errors that plague the simulations with AS-type $K(h)$ functions in silt

830   loam and clay, as they did in silt. Evidently, the AS parameters for the $K(h)$ curve cause numerical problems in fine-textured soils.

4.3 General ramifications

835   We found that 14 out of 18 parameterizations of the soil water retention curve were shown to cause non-physical hydraulic conductivities when combined with the most popular (and effective) class of soil hydraulic conductivity models. For one of these cases (VGN), Ippisch et al. (2006) demonstrated convincingly that their alternative (VGA) significantly improved the quality and numerical efficiency of soil water flow model simulations, and our simulations confirmed the profound effect of this modest modification on the model results. We hope that

840   the general criterion we developed for verifying the physical plausibility of the near-saturated conductivity will be used in the selection of suitable soil hydraulic property parameterizations for practical applications of numerical modeling of water flow in soils, and likewise will be of help in improving existing parameterizations (as we have done in a few cases here) and developing new ones.

The ability of both Burdine's (1953) and Mualem's (1976) models of the soil hydraulic conductivity

845   function to predict independent observations of the soil hydraulic conductivity curve on the basis of soil water retention parameters fitted on water content data only is reasonably good, at least for the limited data available to test this. The conductivity model of Alexander and Skaggs (1986) overestimated the conductivity of the soils for which independent data were available. This resulted in a rapid and unrealistically strong response to changes in atmospheric forcings even at 1 m depth, as shown in our simulation study.

850   The simulations with different parameterizations showed that under the given boundary conditions the choice of the parameterization had a modest effect on evaporation, but strongly affected the partitioning between soil water storage and deep percolation, which in the end determines the water availability to plant roots as well as groundwater recharge. The uncritical use of a default soil hydraulic parameterization or selecting a parameterization solely based on the quality of the fit to soil water retention data points entails the risk of an incomplete appreciation

855   of the potential errors of the water fluxes occurring in the modeled soil. If at all possible, observations during dynamic flow (water contents, matric potentials, fluxes) should be included in the parameterization selection process. In this context it would be interesting to see if parameter-estimation-processes based on inverse modeling of a non-steady unsaturated flow experiment would lead to a different choice of parameterization than fitting

860 parameters to data points obtained at hydrostatic equilibrium. This requires the inclusion of all the parametric expressions of interest in the numerical solvers of Richards' equation capable or running in parameter estimation mode.

865

870

875

880

885

890

895

Code availability

The parameter optimization code is available upon request from G.H. de Rooij. At a later time we intend to make the

900   code available through a website.

905

910

915

920

925

930

Appendix: List of variables

Variables	Dimensions	Properties, and equation to which the variable pertains (where applicable)
A_1	L^{-2}	Constant, Eq. (7)
A_2	-	Constant of, Eq. (12a)
$B(h)$	L^n	Function simplifying notation, Eq. (11c)
b	-	Shape parameter, Eq. (25)
C	-	Constant simplifying notation, Eq. (11c)
c_1	-	Constant, Eq. (14a)
c_2	-	Constant, Eq. (15a)
$\mathbf{d}_\theta$	Varies	Vector of length q_θ of squared differences between observations and fits, Eq. (27)
$E(h)$	$L^{-\kappa}$	Function simplifying notation, Eq. (13e)
F	L^λ	Constant simplifying notation, Eq. (13e)
$F_R(\boldsymbol{x}_{p,R})$	-	Objective function
G	-	Constant simplifying notation, Eq. (16c)
g_0, g_1	-	Fitting parameter, Eq. (19a)
H	L	Sample height
h	L	Matric potential
h_a	L	Matric potential at which the soil reaches the maximum adsorbed water content
h_{ae}	L	Air entry value of the soil
h_c	L	Fitting parameter
h_d	L	Pressure head at oven dryness
h_i	L	Matric potential at the inflection point
h_j	L	Pressure head at junction point
h_m	-	Fitting parameter representing the matric potential at median pore size
h_s	L	Minimum capillary height
I	-	Constant simplifying notation, Eq. (16c)
J	$L^{-\lambda-\kappa}$	Function simplifying notation, Eq (16c)
j	-	Counter
K	$L\,T^{-1}$	Unsaturated hydraulic conductivity
K_s	$L\,T^{-1}$	Saturated hydraulic conductivity
L	-	Constant simplifying notation, Eq. (18c)
M_1	-	Constant simplifying notation, Eq. (18c)

M_2	-	Constant simplifying notation, Eq. (18g)
m	-	Shape parameter of $\theta(h)$
n	-	Shape parameter of $\theta(h)$
$P(h)$	-	Function simplifying notation, Eq. (18c)
R	-	Iteration step
R_{MAX}	-	Maximum number of iteration
S	$L^3 L^{-3}$	Variable running from 0 to S_e
S^{ad}	-	Adsorbed water, Eq. (20)
S^{cap}	-	Capillary water, Eq. (20)
S_e	-	Degree of saturation
T	-	Indicates that the vector is transposed
w	-	Weighting factor ranging between 0 and 1, Eq. (20)
$w_{\theta,R}$	-	Weight factor vector
$w_{R,i}$	-	Individual weighting factor in $w_{\theta,R}$
x	Varies	Integration variable
$\mathbf{x}$	Varies	Parameter vector
$\mathbf{x}_f$	Varies	Vector of non-fitted parameters
$\mathbf{x}_{p,R}$	Varies	Vector of fitted parameters
Y	-	Number of complexes
α	L^{-1}	Shape parameter of $\theta(h)$
β	-	Constant
γ	-	Shape parameter of $K(h)$
ζ_1	-	Constant, Eq. (14a)
ζ_2	-	Constant, Eq. (15a)
η	-	Fitting parameter
θ	$L^3 L^{-3}$	Volumetric water content
θ_a	$L^3 L^{-3}$	Curve fitting parameter representing the volumetric water content when $h = -1cm$
θ_i	$L^3 L^{-3}$	ith observation of the volumetric water content
θ_j	$L^3 L^{-3}$	Volumetric water content at junction point
θ_m	$L^3 L^{-3}$	Water content at h_m
θ_r	$L^3 L^{-3}$	Residual water content
θ_s	$L^3 L^{-3}$	Saturated water content
κ	-	Shape parameter of $K(h)$
λ	-	Fitting parameter of $\theta(h)$

σ		Fitting parameter that characterizes the width of the pore size distribution
$\sigma_{h,i}$, $\sigma_{\theta,i}$	-	Error standard deviations respectively for the ith matric potential and the ith water content
$\sigma^{*}_{h,i}$, $\sigma^{*}_{\theta,i}$	-	Scaled values of $\sigma_{h,i}$, $\sigma_{\theta,i}$
$\sigma^{*}_{i,R}$	-	Scaled standard deviation of (h_i, θ_i) during iteration R
τ	-	Shape parameter of $K(h)$

935

940

945

950

955

960

Author contribution

965

RM gathered the soil hydraulic functions from the literature and carried out the parameter optimization runs with the SCE-based code. RM and GHdR designed the test problem (column size, initial and boundary conditions) for the test simulations with HYDRUS-1D. RM set up, ran, and analyzed these model simulations. GHdR wrote the shell of the optimization code and carried out the mathematical analysis of the soil hydraulic functions. HM carried out the experiments that generated the data used in the paper. JM wrote the SCE parameter optimization code. RM and GHdR wrote the paper. All authors were involved in checking and improving the paper.

970

975

980

985

990

995

References

1000

Alexander, L. and Skaggs, R.W.: Predicting unsaturated hydraulic conductivity from the soil water characteristic, Trans. Am. Soc. Agric. Eng., 29, 176-184, 1986.

Barnes, C.J. and Turner, J.V.: Isotopic exchange in soil water. In: Kendall, C. and McDonell, J.J. (eds.) Isotope tracers in catchment hydrology, pp.137-163. Elsevier, Amsterdam, 839 p, 1998.

1005 Behrangi, A., Khakbaz, B., Vrugt, J.A., Duan,Q and Sorooshian, S.: comment on "dynamically dimensioned search algorithm for computationally efficient watershed model calibration" by Tolson, B.A. and Shoemaker,C. A., Water Resour. Res., 44, doi: 10.1029/2007WR006429, 2008.

Brooks, R.H. and Corey, A.T.: Hydraulic properties of porous media, Colorado State Univ., Hydrology Paper No. 3, 27 pp, 1964.

1010 Burdine, N.T.: Relatvie permeability calculations from pore size distribution data, Trans. Am. Inst. Min. Metall. Pet. Eng., 198, 71-81, 1953.

Campbell, G.S.: A simple method for determining unsaturated hydraulic conductivity from moisture retention data, Soil Sci., 117, 311-314, 1974.

Campbell, G.S., and Shiozawa, S.: Prediction of hydraulic properties of soils using particle-size distribution and
1015 bulk density data. p. 317–328. In: van Genuchten, M.Th., Leij, F.J., and Lund, L.J. (eds.), Indirect methods for estimating the hydraulic properties of unsaturated soils. Univ. of California, Riverside, 1992.

de Vries, J.J. and Simmers, I.: Groundwater recharge: an overview of processes and challenges, Hydrogeology Journal, 10,5-17, doi: 10.1007/s10040-001-0171-7, 2002.

Duan, Q., Sorooshian, S. and Gupta, V.: Effective and efficient global optimization for conceptual rainfall-runoff
1020 models, Water Resour. Res., 28, 1015-1031, 1992.

Durner, W. and Flühler, H.: Soil hydraulic properties. Encyclopedia of Hydrological Sciences, John Wiley & Sons, Ltd, doi: 10.1002/0470848944.hsa077c, 2005.

Fayer, M.J. and Simmons, C.S.: Modified soil water retention functions for all matric suctions, Water Resour. Res., 31, 1233-1238, 1995.

1025 Groenevelt, P.H. and Grant, C.D.: A new model for the soil-water retention curve that solves the problem of residual water contents, European J. of Soil Science, 55, 479-485, doi: 10.1111/j.1365-2389.2004.00617.x, 2004.

Hollenbeck, K.J., and Jensen, K.H.: Maximum-likelihood estimation of unsaturated hydraulic parameters. J. Hydrol., 210, 192-205, 1998.

1030 Hollenbeck, K.J., Šimunek, J. and van Genuchten, M.Th. RETMCL: Incorporating maximum-likelihood estimation principles in the RETC soil hydraulic parameter estimation code, Computers and Geosciences, 26, 319-327, 2000.

Hutson, J.L. and Cass, A.: A retentively functions for use in soil-water simulation models, J. of Soil Sci., 38, 105-113, 1987.

1035   Hoffmann-Riem, H., van Genuchten, M. Th. and Flühler, H.: General model for the hydraulic conductivity of unsaturated soils. In: van Genuchten, M. Th., Leij, F.J. and Wu, L. (eds.), Proceedings of the international workshop on characterization and measurement of the hydraulic properties of unsaturated porous media, Riverside, California, October 22-24, 1997. Part1. U.S. Salinity Laboratory, ARS, U.S. Dept. of Agriculture and Dept. of Environ. Sci., Univ. California, Riverside, California, pp. 31-42, 1999.

1040   Iden, S.C., and Durner, W.: Free-form estimation of soil hydraulic properties using Wind's method. European Journal of Soil Science, 59, 1365-2389, doi: 10.1111/j.1365-2389.2008.01068.x, 2008.

Iden, S.C., and Durner, W.: Comment on 'Simple consistent models for water retention and hydraulic conductivity in the complete moisture range' by Peters, A. Water Resour. Res., 50, 7530-7534, doi: 10.1002/2014WR015937, 2014.

1045   Iden, S.C., Peters, A., and Durner, W.: Improving prediction of hydraulic conductivity by constraining capillary bundle models to a maximum pore size, Adv. Water Resources, 85, 86-92, doi:10.1016/j.advwatres, 2015.09.005, 2015.

Ippisch, O., Vogel, H.-J. and Bastian, P.: Validity limits for the van Genuchten-Mualem model and implications for parameter estimation and numerical simulation, Adv. Water Resources, 29,1780-1789,
1050   doi:10.1016/j.advwatres.2005.12.011, 2006.

Jarvis, N.J., Zavattaro, L., Rajkai, K., Reynolds, W.D., Olsen, P.-A., McGechan, M., Mecke, Mohanty, M. B., Leeds-Harrison, P.B. and Jacques, D.: Indirect estimation of near-saturated hydraulic conductivity from readily available soil information, Geoderma, 108, 1-17, 2002.

Khlosi, M., Cornelis, W.M., Douaik, A., van Genuchten, M. Th. and Gabriels, D.: Performance evaluation of models
1055   that describe the soil water retention curve between saturation and oven dryness, Vadose Zone J., 7, 87-96. doi:10.2136/vzj2007.0099, 2008.

Khlosi, M., Cornelis, W.M., Gabriels, D. and Sin, G.: Simple modification to describe the soil water retention curve between saturation and oven dryness, Water Resour. Res., 42, W11501, doi: 10.1029/2005WR004699, 2006.

1060   Kirkpatrick, S., Gelatt, C. D. and Vecchi, M. P.: Optimization by simulated annealing, Science, 220, 671- 680, doi: 10.1126/science.220.4598.671, 1983.

Klute, A.: Water retention: Laboratory methods. In: Klute, A. (ed.) Methods of soil analysis. Part 1. Physical and mineralogical methods. Second edition. P. 635-662. American Society of Agronomy, Inc, Soil Science Society of America, Inc. Madison, Wisconsin, U.S.A. 1188 pp, 1986.

1065   Kosugi, K.: Lognormal distribution model for unsaturated soil hydraulic properties. Water Resour. Res., 32, 2697-2703, 1996.

Kosugi, K.: General model for unsaturated hydraulic conductivity for soils with lognormal pore-size distribution, Soil Sci. Soc. Am. J., 63, 270-277, 1999.

Lebeau, M. and Konrad, J.- M.: A new capillary and thin film flow model for predicting the hydraulic conductivity
1070   of unsaturated porous media, Water Resour. Res., 46, W12554, doi: 10.1029/2010WR009092, 2010.

Liu, H.H., and Dane, J.H.: Improved computational procedure for retention relations of immiscible fluids using pressure cells, Soil Sci. Soc. Am. J., 59, 1520-1524, 1995.

Mualem, Y.: A new model for predicting the hydraulic conductivity of unsaturated porous media, Water Resour. Res., 12, 513-521, 1976.

1075 Mualem, Y.: Modeling the hydraulic conductivity of unsaturated porous media, p. 15–36. In: van Genuchten, M.Th., Leij, F.J., and Lund, L.J. (eds.), Indirect methods for estimating the hydraulic properties of unsaturated soils. Univ. of California, Riverside, 1992.

National centers for environmental information: http://www.ncdc.noaa.gov/cdo-web/, last Access: 1 March 2016.

Olver, F.W.J., Lozier, D.W., Boisvert, R.F and Clark, C.W. (Editors): NIST Handbook of mathematical
1080 functions. National Institute of Standards and Technology (U.S. Dept. of Commerce), and Cambridge University Press, Cambridge, UK, 2010.

Peters, A.: Simple consistent models for water retention and hydraulic conductivity in the complete moisture range, Water Resour. Res., 49, 6765-6780, doi:10.1002/wrcr.20548, 2013.

Peters, A.: Reply to comment by Iden, D. and Durner, W. on 'Simple consistent models for water retention and
1085 hydraulic conductivity in the complete moisture range.' Water Resour. Res., 50, 7535-7539, doi: 10.1002/2014WR016107, 2014.

Peters, A., and Durner, W.: Simplified evaporation method for determining soil hydraulic properties, J. Hydrol., 356, 147–162, 2008.

Press, W.H., Teukolsky, S.A., Vetterling, W.T., and Flannery, B.P.: Numerical recipes in Fortran. The art of
1090 scientific computing. 2nd ed., Cambridge University Press, Cambridge, UK, 1992.

Raats, P.A.C.: A superclass of soils. p. 45–51. In: van Genuchten, M.Th., Leij, F.J., and Lund, L.J. (eds.), Indirect methods for estimating the hydraulic properties of unsaturated soils. Univ. of California, Riverside, 1992.

Rossi, C., and Nimmo, J.R.: Modeling of soil water retention from saturation to oven dryness, Water Resour. Res., 30, 701-708, 1994.

1095 Scanlon, B.R., Keese, K.E., Flint, A.L., Flint, L.E., Gaye, C.B., Edmunds, W. M. and Simmers, I.: Global synthesis of groundwater recharges in semiarid and arid regions, Hydrological Processes, 20, 3335-3370, doi: 10.1002/hyp.6335, 2006.

Schaap, M.G., and Leij, F.J.: Improved prediction of unsaturated hydraulic conductivity with the Mualem-van Genuchten model, Soil Sci. Soc. Am. J., 64, 843-851, 2000.

1100 Schaap, M.G., and van Genuchten, M. Th.: A modified Mualem-van Genuchten formulation for improved description of the hydraulic conductivity near saturation, Vadose Zone J., 5, 27-34, doi:10.2136/vzj2005.0005, 2006.

Schelle, H., Heise, L., Jänicke, K., and Durner, W.: Water retention characteristics of soils over the whole moisture range: a comparison of laboratory methods, European Journal of Soil Science, 64, 814 – 821, 2013.

1105 Schindler, U., von Unold, G., Durner, W., and Mueller, L.: Recent progress in measuring soil hydraulic properties, In: Proceedings of the International Conference on Environment and Civil Engineering, April 24-25, 2015, Pattaya, Thailand, p. 47-52, doi:10.15242/IAE.IAE0415401, 2015.

Šimůnek, J. Šejna, M., Saito, H., Sakai, M., and Th. van Genuchten, M.: The HYDRUS-1D software package for simulating the one-dimensional movement of water, heat, and multiple solutes in variably-saturated media, 2013.

Tolson, B.A. and Shoemaker, C. A.: Dynamically dimensioned search algorithm for computationally efficient watershed model calibration, 43, W01413, doi: 10.1029/2005WR004723, 2007.

Tuller, M. and Or, D.: Hydraulic conductivity of variably saturated porous media: Film and corner flow in angular pore space. Water Resour. Res., 37, 1257-1276, doi: 10.1029/2000WR900328, 2001.

UNDP: Human Development Report 2006. Beyond scarcity: power, poverty and the global water crisis, United Nations development programme, New York, 422 pp., 2006.

UN-Water, FAO: Coping with water scarcity. Challenge of the twenty-first century, 29 pp., 2007.

van Genuchten, M.Th.: A closed-form equation for predicting the hydraulic conductivity for unsaturated soils, Soil Sci. Soc. Am. J., 44, 892-898, 1980.

Vogel, T., van Genuchten, M.Th. and Cislerova, M.: Effect of the shape of the soil hydraulic functions near saturation on variably-saturated flow predictions, Adv. Water Resour, 24, 133-144, 2000.

Tables:

Table 1: The fitting parameters for five parameterizations, their physically permitted ranges, and their fitted values for four textures. The three-character parameterization label is explained in the main text. The equations to which these labels refer are given in the first column.

1140

Parameter-ization	Fitted parameter	Unit	Range	Texture Silt	Sand	Clay	Silt loam
BCO Eq. (5a)	θ_r	-	$0 - \theta_s$	0.000127	0.013300	0.000004	0.000015
	θ_s	-	$\theta_r - 1$	0.445	0.366	0.516	0.358
	h_{ae}	cm	$-\infty - 0$	-21.426	-7.161	-50.577	-30.440
	λ	-	$0 - \infty$	0.197	0.520	0.091	0.163
FSB Eq. (16a)	θ_s	-	$\theta_a - 1$	0.449	0.366	0.519	0.358
	θ_a	-	$0 - \theta_s$	0.177	0.048	0.500	0.312
	h_{ae}	cm	$h_d - 0$	-11.537	-11.508	-16.783	-11.668
	λ	-	$0 - \infty$	0.254	0.719	0.152	0.364
RNA Eq. (13a)	θ_s	-	$0 - 1$	0.460	0.382	0.522	0.358
	h_{ae}	cm	$h_j - 0$	-2.826	-1.884	-50.856	-30.250
	h_j	cm	$h_d - h_{ae}$	-2876	-359000	-49.882	-11641
VGA Eq. (11a)	θ_r	-	$0 - \theta_s$	0.000133	0.012880	0.000019	0.000041
	θ_s	-	$\theta_r - 1$	0.461	0.366	0.514	0.358
	α	cm^{-1}	$0 - \infty$	0.0197	0.8391	0.0055	0.0093
	n	-	$1 - \infty$	1.252	1.511	1.127	1.219
	h_{ae}	cm	$-\infty - 0$	-0.0015	-6.4626	-47.2530	-0.0081
VGN Eq. (8a)	θ_r	-	$0 - \theta_s$	0.000025	0.013560	0.001160	0.000003
	θ_s	-	$\theta_r - 1$	0.461	0.370	0.509	0.360
	α	cm^{-1}	$0 - \infty$	0.0200	0.1353	0.0042	0.0095
	n	-	$1 - \infty$	1.251	1.528	1.127	1.219

1145

Table 2: Root mean square of errors (RMSE) for the different parameterizations.

| Parameterization | Texture | | | |
	Silt	Sand	Clay	Silt loam
BCO	0.1422	0.1164	0.1858	0.1122
FSB	0.1248	0.1163	0.1205	0.1068
RNA	0.0341	0.0130	0.2192	0.1101
VGA	0.0118	0.1164	0.1604	0.0412
VGN	0.0118	0.0111	0.1547	0.0411

1150

1155

1160

1165

Table 3: Cumulative bottom and evaporative fluxes (positive upwards) for silt from day 281 (the start of the first rainfall) onwards for Burdine and Mualem conductivity functions with the different parameterizations. The hydraulic conductivity at $h = -300$ cm (the initial condition at the bottom is also given).

	Cumulative bottom flux (cm)		Cumulative evaporation (cm)		$K(-300)$ (cm d^{-1})
Parameterization	Burdine	Mualem	Burdine	Mualem	Mualem
BCO	-0.70	-0.500	34.147	34.445	0.00080
FSB	-1.240	-0.910	33.219	33.736	0.00147
RNA	-4.337	-3.650	27.046	28.184	0.00702
VGA	-	-0.248	-	34.956	0.00014
VGN	-	-0.744	-	34.359	0.00119

1170

1175

1180

1185

Figures:
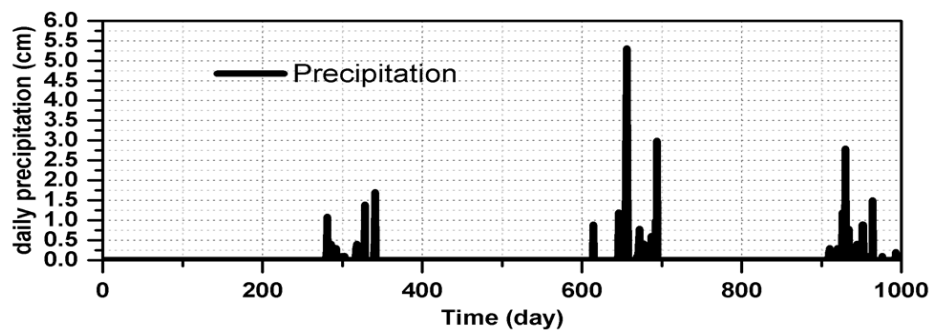
1190

Figure 1: The record of daily rainfall sums from Riyadh city that was used in the numerical scenario study. Three rainfall clusters are visible. The largest daily rainfall amount (5.4 cm) fell on day 656. The observation period starts at June 4, 1993, and ends at February 27, 1996.

1195

1200
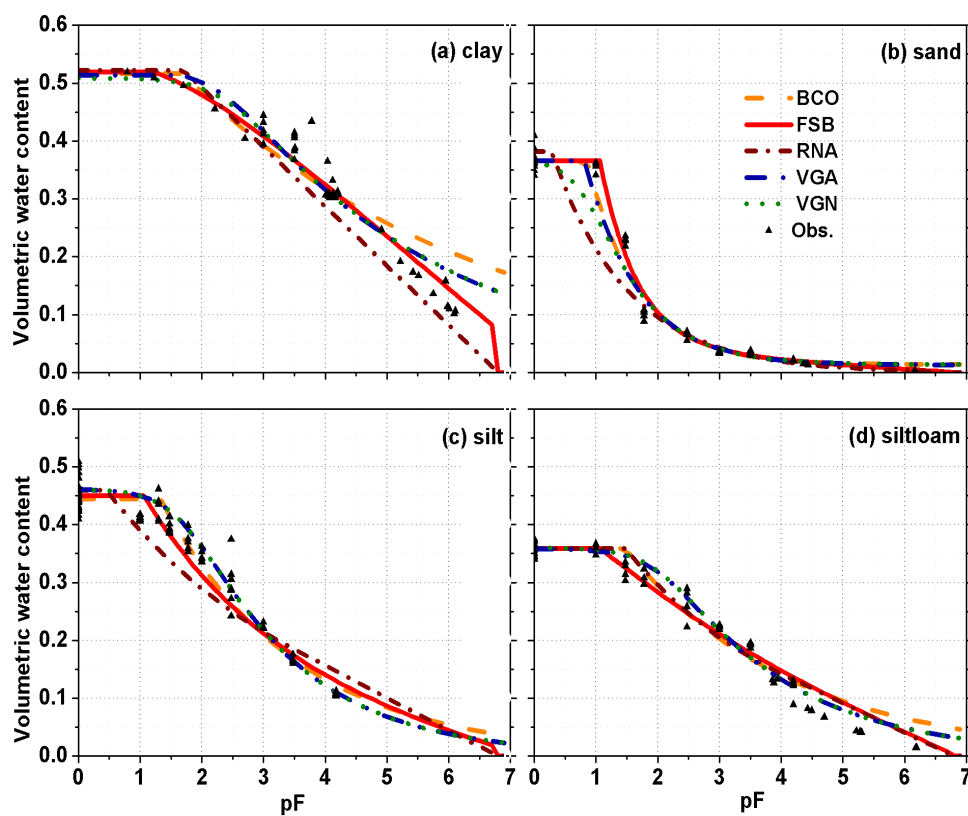
Figure 2: Observed and fitted retention curves for the different soil textures.
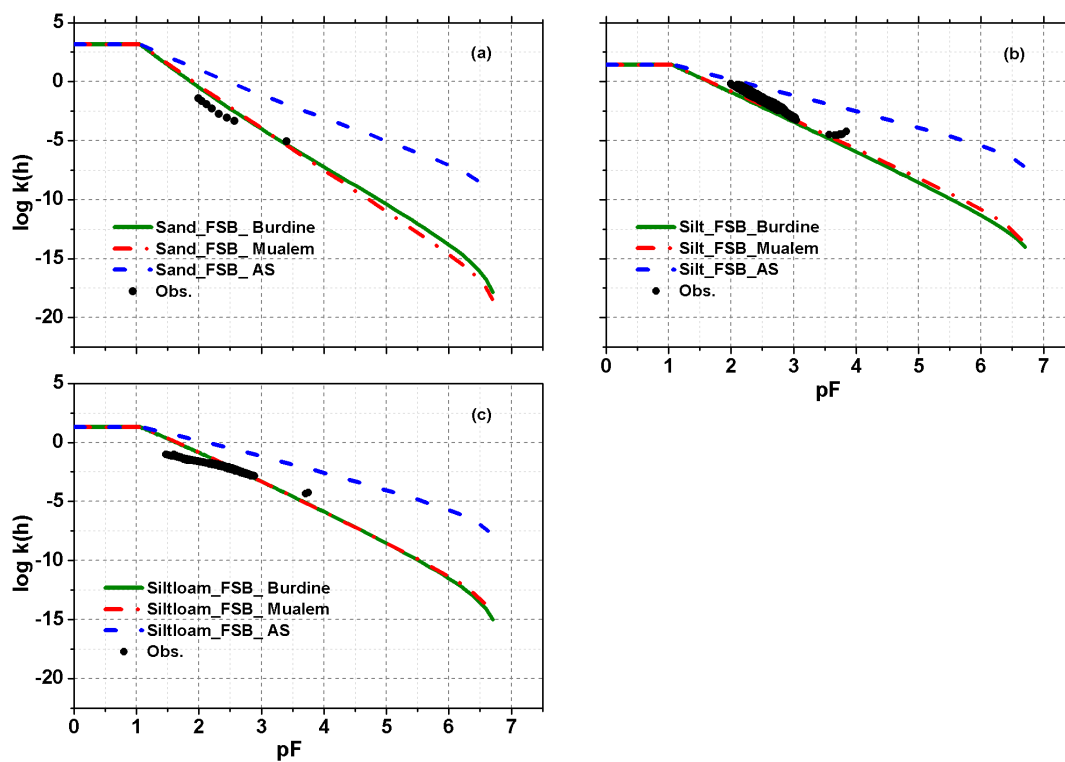
Figure 3: The observed and fitted hydraulic conductivity curve according to Burdine (1953), Mualem (1976) and Alexander and Skaggs (1986) using the fitted parameters of the Fayer and Simmons soil water retention curve (1995) for (a) sand, (b) silt, and (c) silt loam.
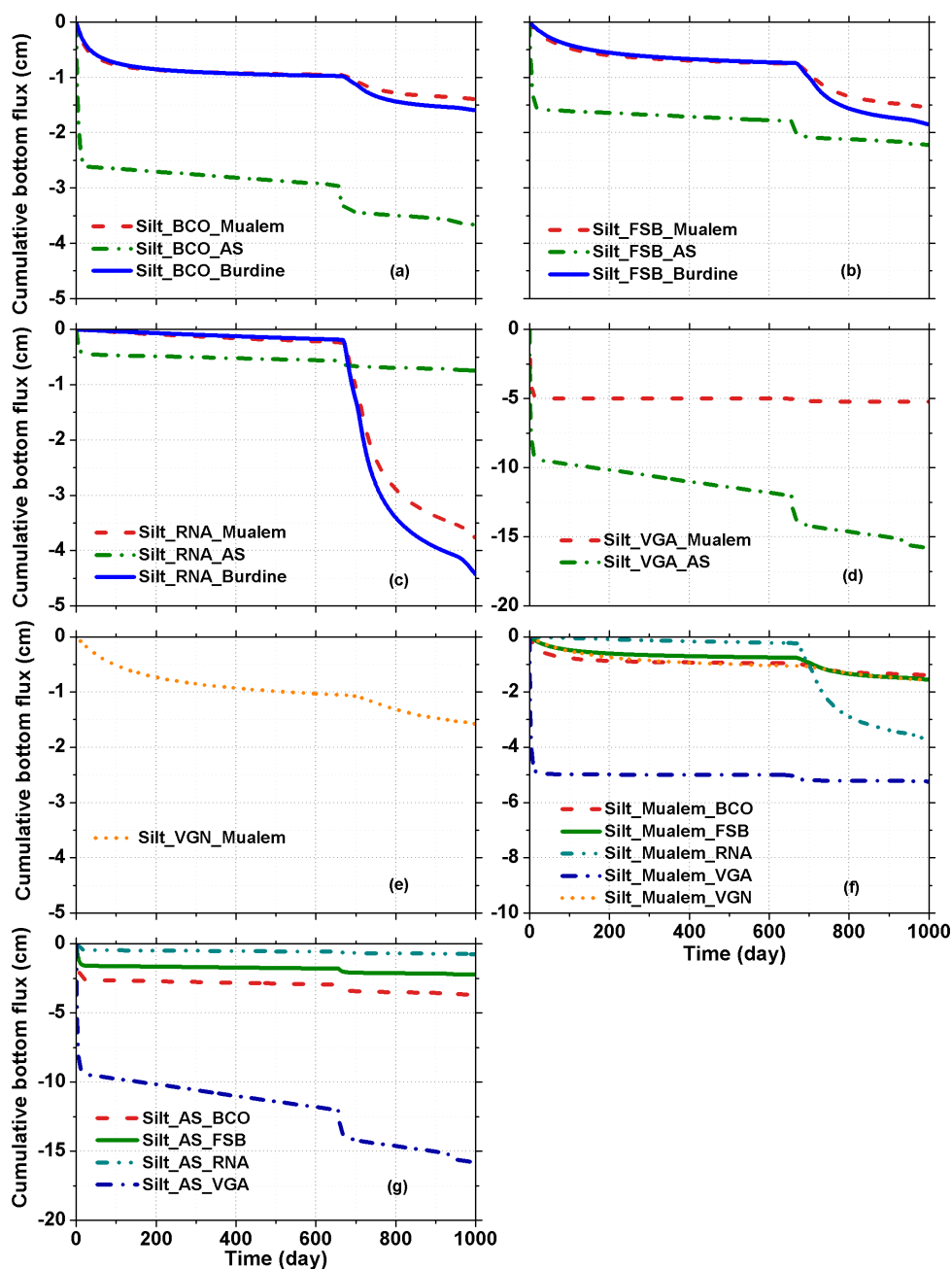
1210

Figure 4: The cumulative bottom fluxes leaving a silt soil column for the different combinations of soil water retention curve and hydraulic conductivity parameterizations. Panels a through e present the results for the indicated retention parameterizations (see Table 1). Panels f and g organize the results according to the conductivity function: either Mualem (1976) (f) or Alexander and Skaggs (1986) (g).
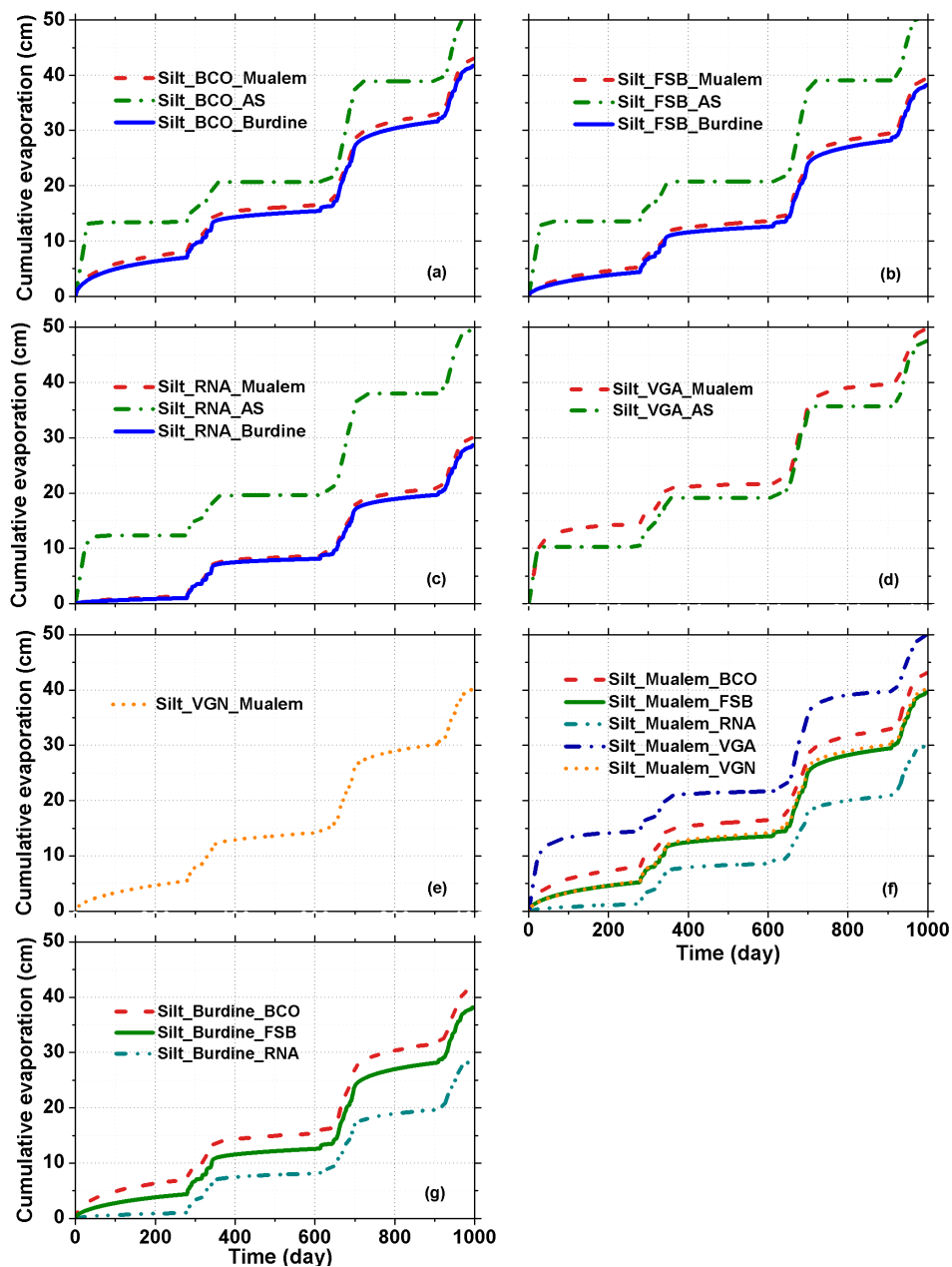
Figure 5: Cumulative evaporation from a silt soil column for the different combinations of soil water retention and hydraulic conductivity parameterizations. Panels a through e present the results for the indicated retention parameterizations (see Table 1). Panels f and g organize the results according to the conductivity function: either Mualem (1976) (f) or Burdine (1953) (g).

1215
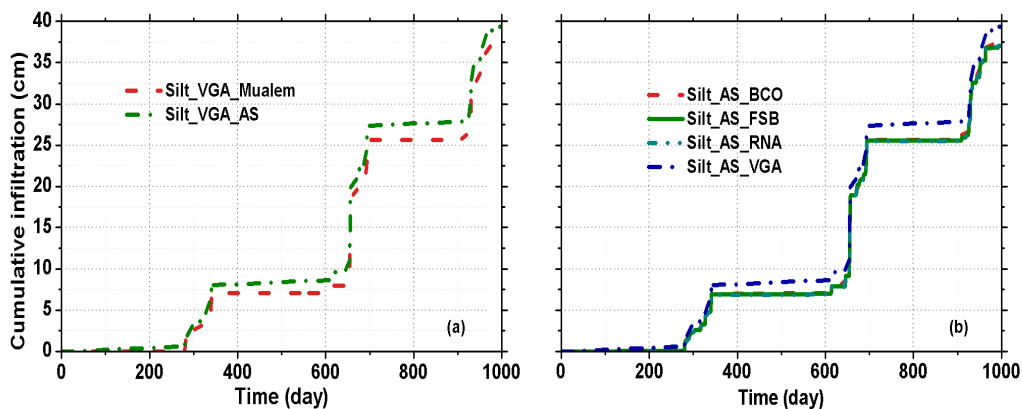
1220

Figure 6: Cumulative infiltration in a silt profile for the VGA parameterization (see Table 1) with conductivity functions according to Mualem (1976) and Alexander and Skaggs (1986) (a) and four different parameterizations for the retention curve (see Table 1) with the Alexander and Skaggs conductivity function (b).
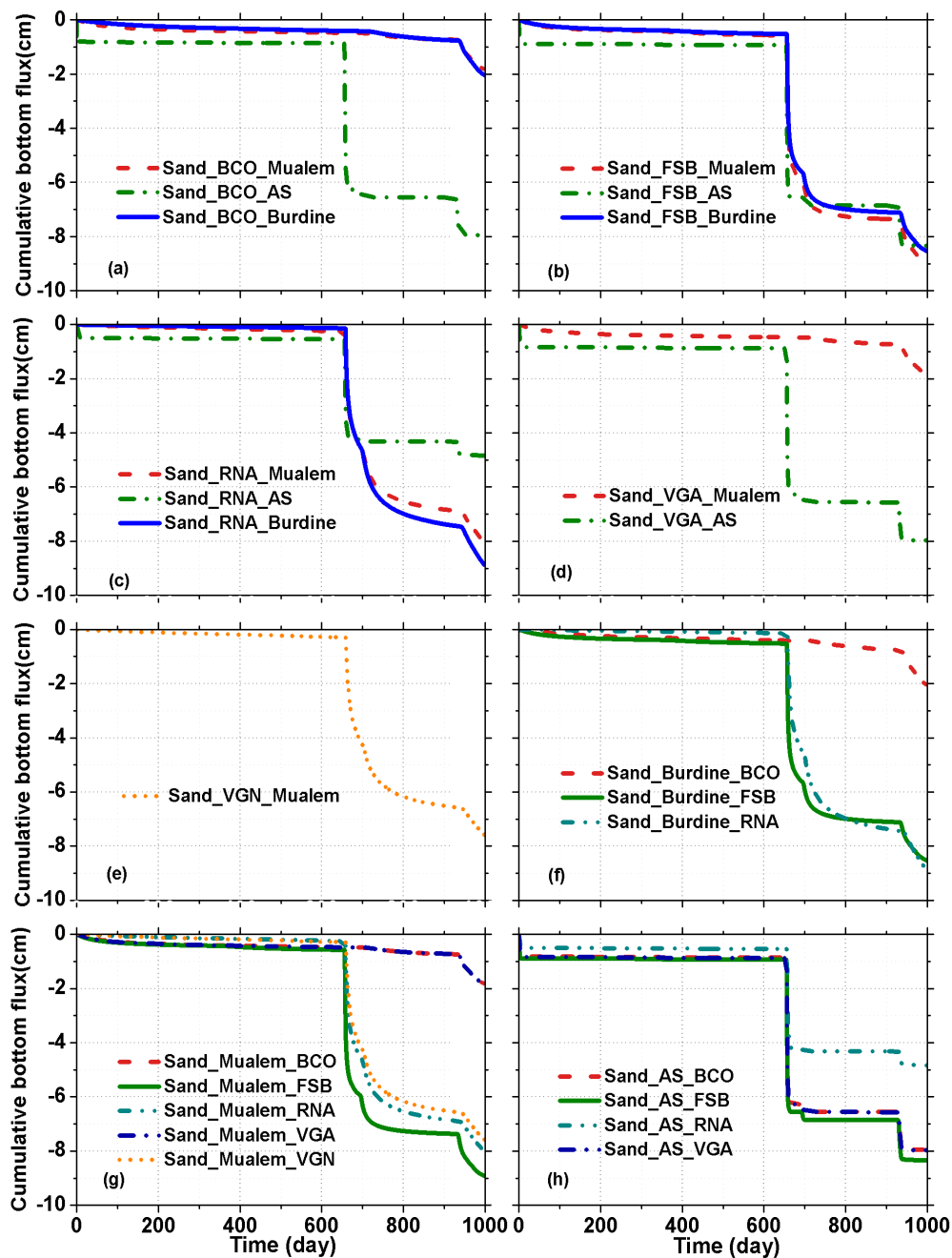
1225   Figure 7: As Fig. 4, but for a sandy soil column. Unlike Fig. 4, the results of Burdine's (1953) conductivity curve are shown (panel f).
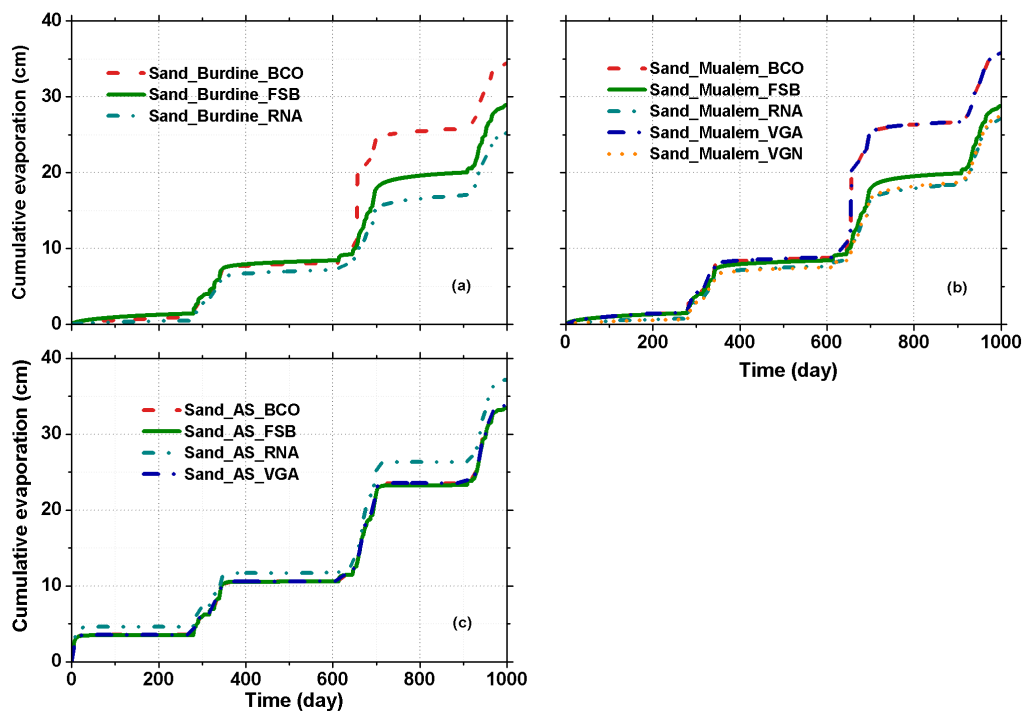
Figure 8: Cumulative evaporation from a sandy profile for the different combinations of retention curve parameterizations (see Table 1) and hydraulic conductivity functions: Burdine (1953) (a), Mualem (1976) (b) or Alexander and Skaggs (1986) (c).

1230
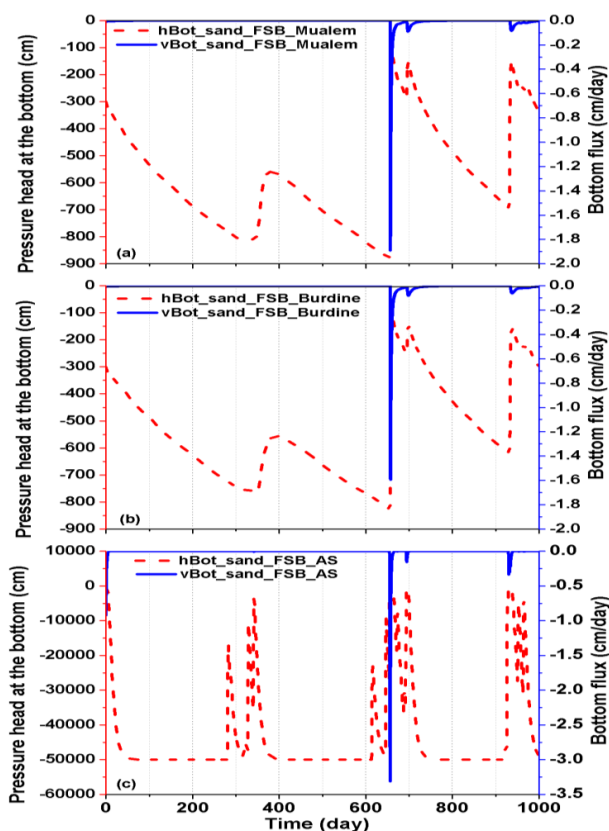
Figure 9: Pressure head hBot and flux density vBot at the bottom of the sand column for the FSB parameterization (see Table 1) and the conductivity functions of Mualem (1976) (a), Burdine (1953) (b) and Alexander and Skaggs (1986) (c).

1235
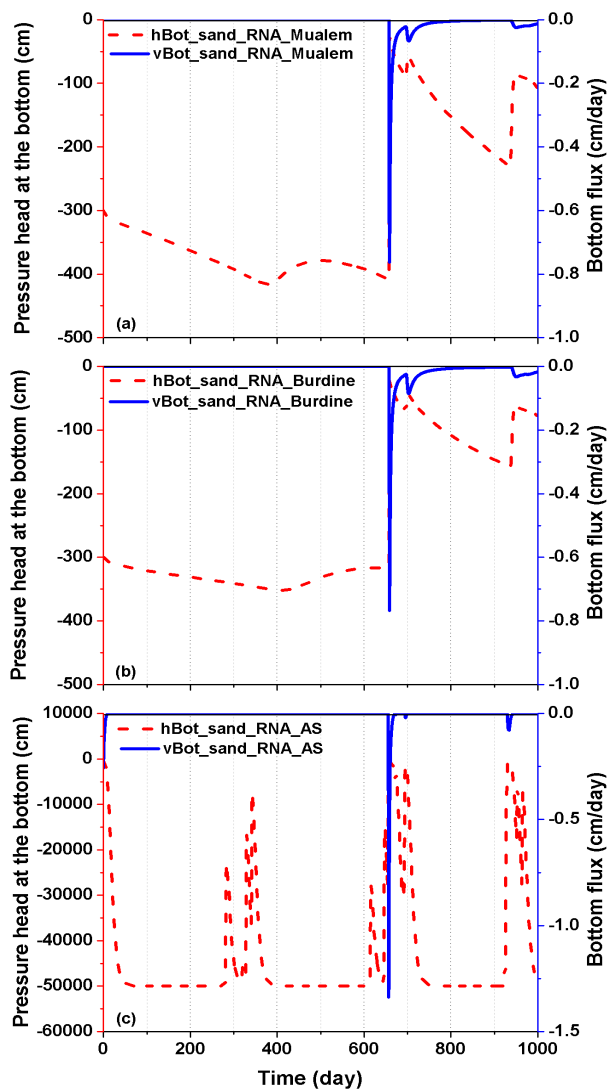
Figure 10: As Figure 9, but for the RNA parameterization (see Table 1).
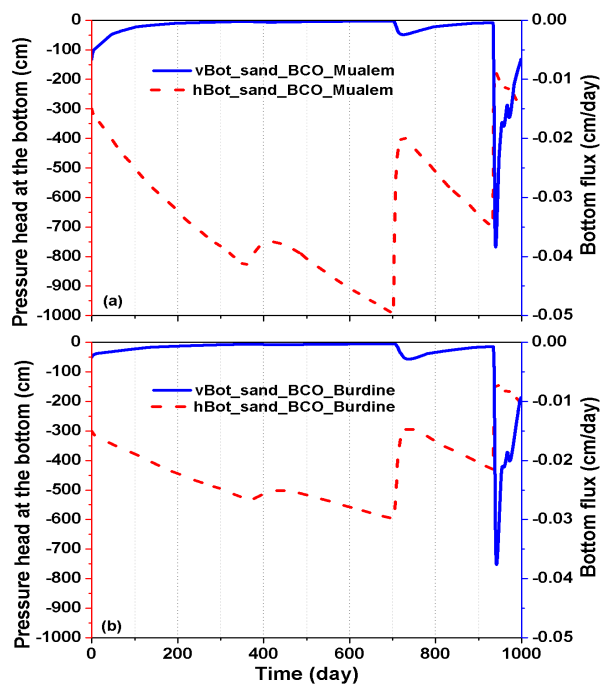
1240

Figure 11: As Figure 9, but for the BCO parameterization (see Table 1).
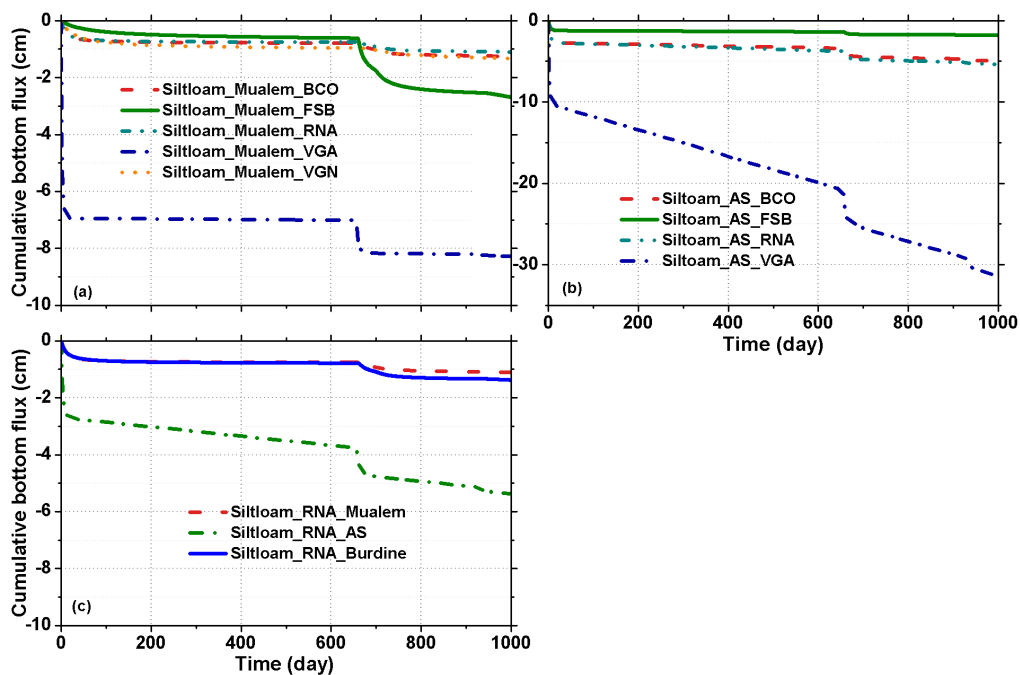
Figure 12: Cumulative bottom fluxes from a silt loam profile for all combinations of parameterizations (see Table 1) and Mualem's (1976) (a) and Alexander and Skaggs' (1986) conductivity functions (b), and for the RNA parameterization with all three conductivity functions (c).
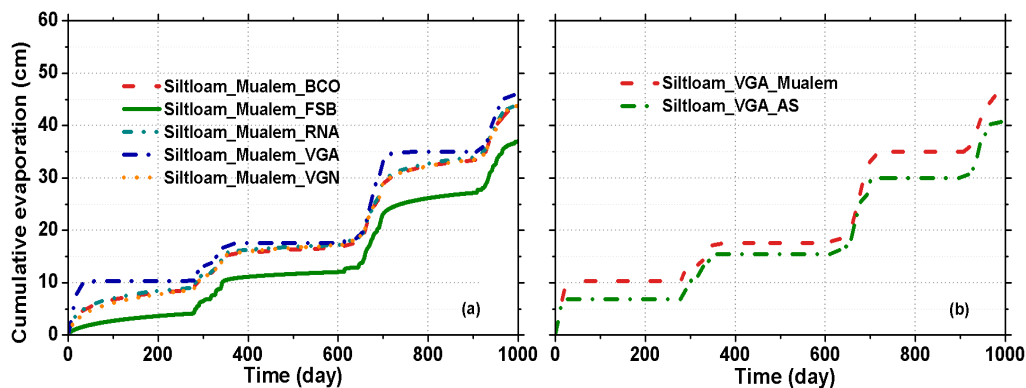
Figure 13: Cumulative evaporation from a silt loam profile for all parameterizations (see Table 1) with Mualem's (1976) conductivity function (a) and the VGA parameterization with conductivity functions according to Mualem (1976) and Alexander and Skaggs (1986) (b).
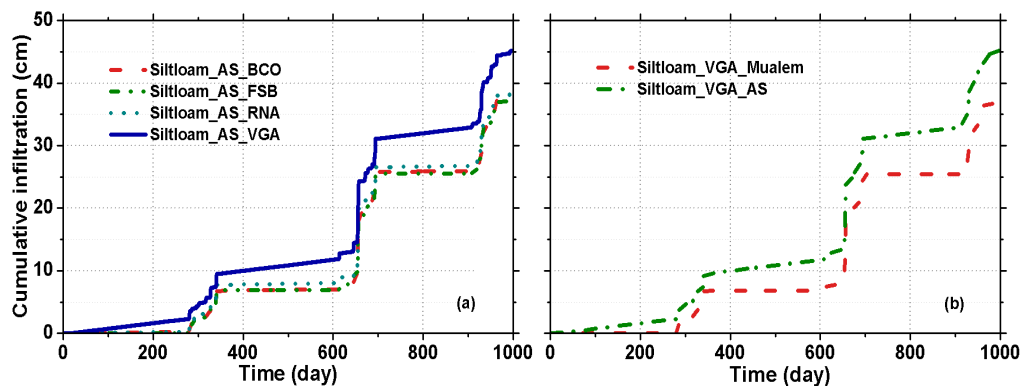
Figure 14: Cumulative infiltration from a silt loam profile for four parameterizations (see Table 1) with the Alexander and Skaggs (1986) conductivity function (a) and for the VGA parameterizations with conductivity functions according to Mualem (1976) and Alexander and Skaggs (1986) (b).

1275

1280
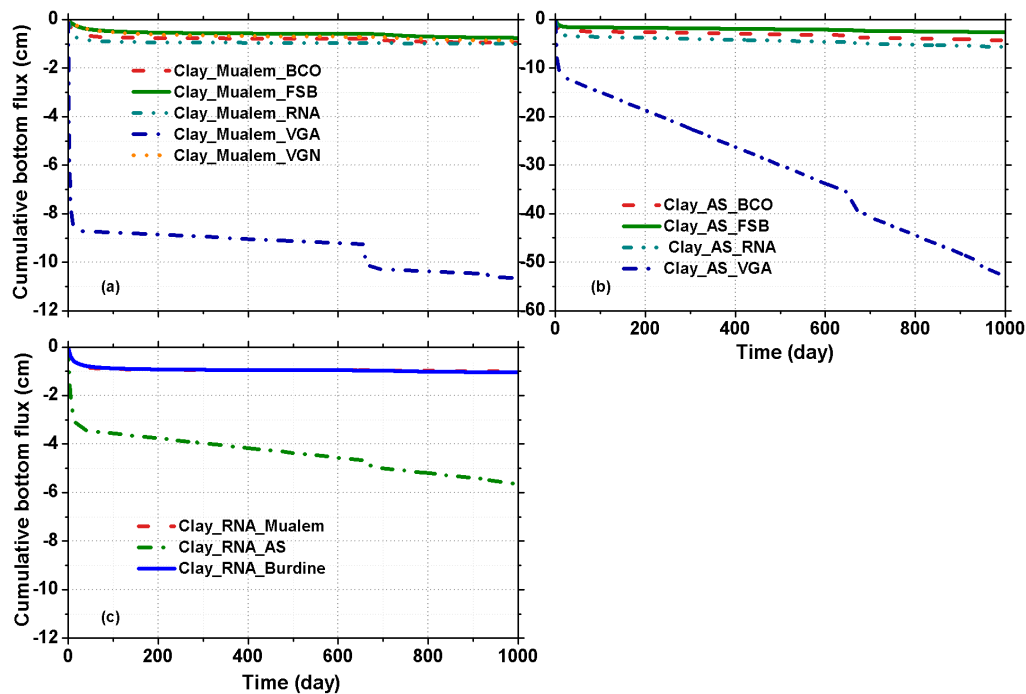
Figure 15: As Fig. 12, for clay.

1285

1290
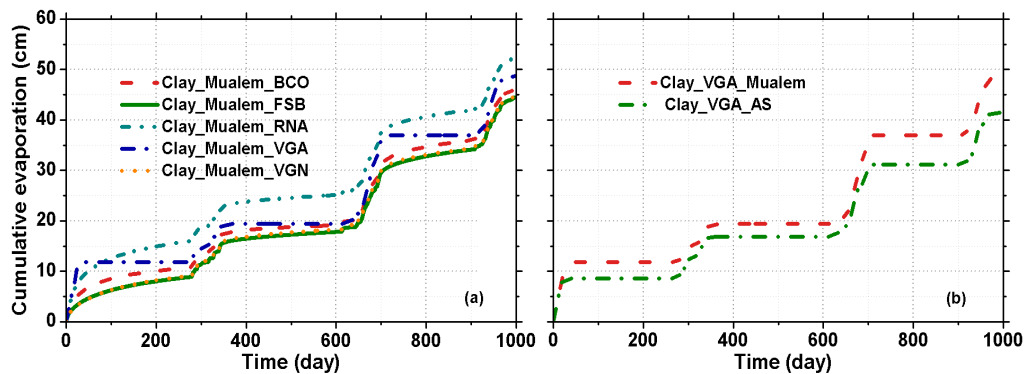
Figure 16: As Fig. 13, for clay.

1295

1300

1305

1310
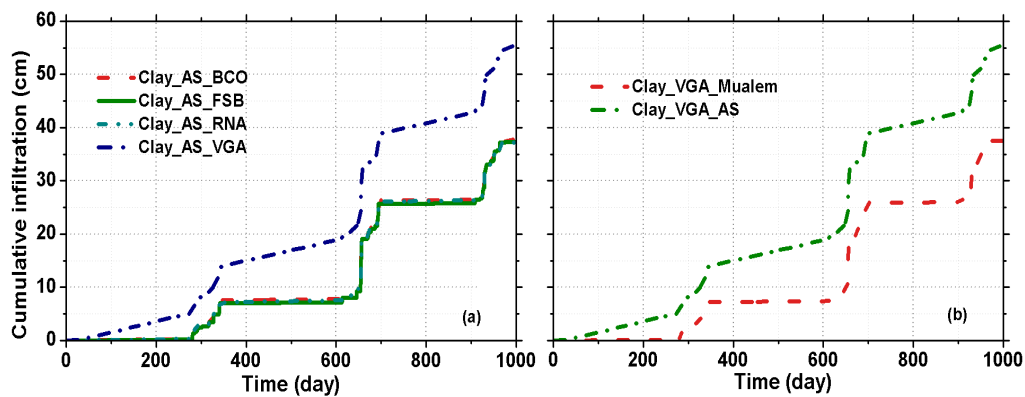
Figure 17: As Fig. 14, for clay.

1315